ICARUS **122,** 406–427 (1996)
ARTICLE NO. 0133

Origin of the Spacewatch Small Earth-Approaching Asteroids

WILLIAM F. BOTTKE, JR.

Division of Geological and Planetary Science, California Institute of Technology, 170-25, Pasadena, California 91125
E-mail: bottke@kepler.gps.caltech.edu

MICHAEL C. NOLAN

Arecibo Observatory, P.O. Box 995, Arecibo, Puerto Rico 00613

AND

H. JAY MELOSH, ANN M. VICKERY, AND RICHARD GREENBERG

Lunar and Planetary Laboratory, University of Arizona, Tucson, Arizona 85721

Received June 19, 1995; revised November 27, 1995

Recent discoveries of small Earth-approaching asteroids by the 0.9 m Spacewatch telescope (referred to here as S-SEAs) reveal 16 objects which have diameters ~50 m or smaller. Approximately half of these objects lie in a region where few large near-Earth asteroids are found, with perihelia (q) and aphelia (Q) near 1 AU, $e < 0.35$, and i from 0° to ~30°. Possible origins for these objects are examined by tracking the orbital evolution of test bodies from several possible source regions using an Öpik-type Monte Carlo dynamical evolution code, modified to include (a) impact disruption, based on a map in orbital (a, e, i) space of collision probabilities and mean impact velocities determined using actual main-belt and near-Earth asteroid orbits, (b) fragmentation, and (c) observational selection effects.

Amor asteroid fragments evolving from low eccentricity Mars-crossing orbits beyond the $q = 1$ AU line provide a reasonable fit to S-SEA orbital data. Planetary ejecta from Mars is only consistent with low and moderately inclined S-SEA orbits. Asteroidal fragments from the main-belt via the 3:1 or ν_6 chaotic resonance zones rarely achieve low-e orbits before planetary impacts, comminution, or ejection remove them from the system. This source could produce the observed moderate-to-high eccentricity S-SEAs. Plantary ejecta from the Earth–Moon system and Venus are only consistent with low-inclination S-SEA orbits. Moreover, constraints set by the planetary cratering record and the meteorite record suggest that the Earth, Moon, and Venus are unlikely to provide many S-SEAs. All of these results are predicated on the observational bias computations (Rabinowitz, D.L. 1994. *Icarus* 111, 364–377) that provide the current definition of the S-SEA population.

I. INTRODUCTION

A substantial fraction of near-Earth asteroids (NEAs) are thought to be fragments from main-belt asteroid collisions which reach Earth-crossing or near Earth-crossing orbits via a chaotic resonance zone (e.g., the 3:1 mean-motion resonance with Jupiter, the ν_6 secular resonance). However, many factors complicate this scenario: (a) short-period comets frequent some of the same regions as NEAs, making it possible that "extinct" comets provide a partial source for NEAs (Wetherill 1985, 1988). (b) Perturbations caused by the terrestrial planets and resonances caused by the jovian planets both scatter NEAs, making it difficult to determine their point of origin. (c) NEAs are products of comminution due to collisions, so a single disruption event could create a population of smaller objects in a relatively empty region for an extended amount of time. (d) Not all asteroids are from the main belt, e.g., some Antarctic meteorites and SNC meteorites probably came from the Moon and Mars, respectively. Distinct sub-populations of NEAs may have their own source regions. Such populations may be characterized by being dynamically or spectrally distinctive. Proposed models of their origins must also be consistent with the size–frequency distribution of the sub-population and must take into account selection effects that affect their distribution and how long they can remain distinctive before they are scattered.

Here we investigate possible sources of a putative sub-population of NEAs identified by Rabinowitz *et al.* (1993): a set of bodies discovered by the Spacewatch project, comprising 16 of the smallest NEAs (diameter $D \leq 50$ m) ever observed. Orbits of these "Spacewatch small-Earth approachers" (S-SEAs) are shown in Fig. 1 and Table I. Half of these bodies lie in a region where few larger NEAs have previously been found, specifically with perihelia (q) near 1 AU, eccentricities $e < 0.35$, and inclinations i from 0° to ~30°. Rabinowitz *et al.* claim there is an excess of

0019-1035/96 $18.00

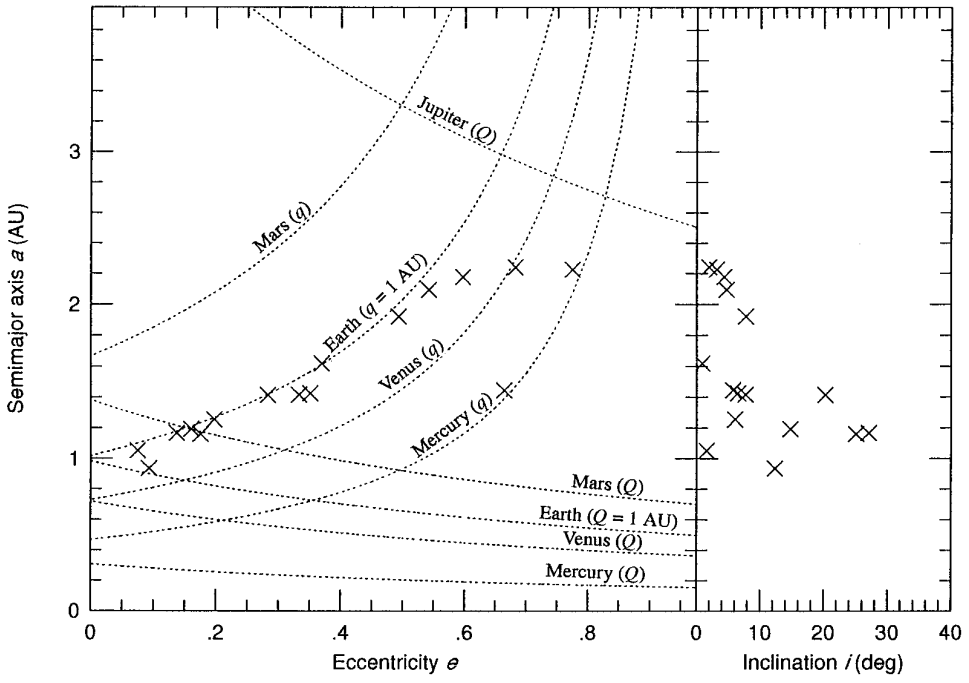

FIG. 1. Plot showing the positions of the small Spacewatch Earth-approaching asteroids (S-SEAs) in (a, e) and (a, i) space (shown by the crosses). The objects characterizing the excess population have low eccentricity orbits ($e < 0.35$) and perihelia (q) which barely cross the orbit of the Earth. The dotted lines show where the asteroids have perihelia (q) or aphelia (Q) crossing the orbits of Jupiter or the terrestrial planets. Thus, asteroids with (a, e) positions between those lines cross that planet's orbit.

TABLE I
Orbital Elements and Brightness for the Spacewatch Small Earth-Approaching Asteroids[a]

Name	a	e	i	Ω	ω	M	H	Type
1991 BA	2.243	0.682	1.961	118.343	70.582	343.253	28.0	Apollo
1991 TT	1.193	0.161	14.762	191.814	217.773	321.237	26.0	Amor
1991 TU	1.416	0.333	7.681	192.837	220.945	330.349	28.0	Apollo
1991 VA	1.426	0.351	6.505	36.999	313.302	21.780	27.0	Apollo
1991 VG	1.051	0.075	1.590	78.921	26.523	335.421	28.0	Apollo
1992 DU	1.160	0.175	25.062	337.297	121.645	43.587	25.0	Apollo
1992 YD_3	1.166	0.137	27.042	273.640	173.729	331.142	26.0	Apollo
1993 BD_3	1.618	0.369	0.867	313.056	168.346	5.116	26.0	Amor
1993 DA	0.936	0.093	12.332	328.601	354.490	191.461	26.0	Aten
1993 FA_1	1.414	0.283	20.221	186.684	343.338	12.646	26.0	Amor
1993 HD	1.445	0.664	5.740	201.793	253.088	23.533	25.0	Apollo
1993 HP_1	1.921	0.493	7.775	36.401	151.885	6.954	27.0	Apollo
1993 KA	1.255	0.198	6.055	235.186	341.875	65.205	26.0	Amor
1993 KA_2	2.227	0.775	3.188	238.824	261.409	35.108	29.0	Apollo
1993 TZ	2.179	0.597	4.361	203.044	231.374	349.500	26.0	Apollo
1993 UA	2.094	0.542	4.694	26.499	329.945	7.618	26.0	Apollo

[a] This table lists the B1950 orbital elements in the following order: semimajor axis a (AU), eccentricity e, inclination i (°), longitude of ascending node Ω (°), argument of perihelion ω (°), and mean anomaly M (°). The absolute magnitude H and the NEA type are also shown.

small bodies relative to their expectation based on the small number of larger bodies ($D > 100$ m) there.

Other results suggest the S-SEAs may not be a distinct population; Jopek *et al.* (1995) found that fireballs, bodies roughly the same size as S-SEAs which glow brightly from frictional heating when they enter the atmosphere, follow the same type of evolutionary paths followed by larger NEAs, implying that the S-SEA population may not be large or dynamically distinct. However, the selection effects for fireballs are much different than those for the S-SEAs, making a direct comparison difficult.

If Rabinowitz's excess population is real, it has important implications for the provenance of NEAs and meteorites. This small-body excess could be caused by the particular collisional and dynamical evolution of objects found in the S-SEA orbital region (Farinella and Davis 1994), or, alternatively, by evolution from some distinct source. To investigate this, we explore possible source regions for the S-SEAs, including the main belt, the terrestrial planets, and other NEAs.

Any potential source must be consistent with the following constraints: (1) the known S-SEA orbits, (2) S-SEA spectra, (3) the paucity of special meteorites (e.g., martian or lunar meteorites) relative to the overall meteorite record and the special meteorite record itself, and (4) the frequency of impact events that could create the observed S-SEAs. However, since the quality of S-SEA spectra is quite poor at the time of this writing, it is not currently a useful constraint.

II. THE MODEL

II.A. The Monte Carlo Code

To determine which of the above sources are viable, we track test bodies as they dynamically evolve from each source using the Monte Carlo dynamical evolution code of Melosh and Tonks (1993), which was based on the earlier work of Öpik (1951), Arnold (1965), and Wetherill (1985, 1988). This code computes the probability that a given test body will encounter one of the terrestrial planets, but does not actually integrate the orbit of each body. It assumes that both the planets and the test bodies are on independent keplerian orbits with uniformly precessing apsides and nodes around the Sun. They are considered unperturbed unless they enter a planet's sphere of influence, where they either (a) collide with the planet or (b) experience a ΔV based on a two-body encounter model, which alters the orbit of the test body. This process is repeated until the test body impacts a planet, is disrupted by an asteroid collision, or is ejected from the system through a close approach with a jovian planet.

This model also makes several assumptions to speed computation time:

Assumption 1. Particle-in-a-box approximations and random scatterings, based on gas dynamics, give approximate encounter frequencies. Wetherill (1967) compared the particle-in-a-box method with the more detailed calculation method of Öpik (1951). He showed that the particle-in-a-box method was a useful approximation for most applications, although errors could be a factor of two or more.

Assumption 2. Two-body scattering is applicable to all encounters. This approximation was tested by Bottke (1995), who assessed the accuracy of Monte Carlo results by developing a numerical model which tracked test bodies on heliocentric orbits encountering a planet. Their results showed that the outcome statistics of Monte Carlo codes yield reasonable outcome statistics (relative to numerical integration) even in low velocity regimes where pathological behavior is common. By testing large particle swarms encountering a planet, they found that some test bodies, whose approach orbits were shifted onto different trajectories by distant planetary perturbations, were replaced by similarly shifted nearby test bodies. This type of ''particle replacement'' by a population of test bodies preserves outcome statistics in a Monte Carlo model relative to numerical integration results (Greenberg *et al.* 1988). Consequently, a population of test bodies preserves two-body outcome statistics as long as a large number of bodies (with a range of orbital parameters) encounter the planet. Milani *et al.* (1990) found similar agreement when they compared the numerically integrated orbits of the known NEAs with the encounter statistics of Wetherill's (1967) model, as did Gladman *et al.* (1995).

Assumption 3. Effects of non-collision encounters within the sphere of influence can be approximated by a small number of encounters through the use of a so-called ''K'' factor defined by Arnold (1965). The K factor approximation works in the following way: Only encounters within a target circle of radius $K\tau$ are considered directly (τ is the gravitational cross section radius of the planet). Each test body entering this target circle is assigned a random approach distance to go along with its predetermined encounter velocity. The probability of encounter on the outer half of the target circle (i.e., at distances greater than $(K\tau)/2$)) is increased by a correction factor to account for the large number of distant encounters which occur outside the target circle but inside the sphere of influence, assuming that these encounters behave as a random walk. An encounter on the outer half of the target circle produces a moderate change (i.e., ΔV) in the orbit of the test body. Approaches on the inner half of the target circle produce even larger ΔV's or a planetary impact. Thus, the K value allows one to trade computational expediency for accuracy. The value used in these simulations, $K = 10$, was found to be satisfactory by both Arnold (1965) and Melosh and

Tonks (1993). The K factor approximation was also tested by Nolan (1994), who determined that a finite interaction zone approximation from the sphere of influence and Arnold's K factor introduced errors on the order of 20–40% (smaller than the particle-in-a-box error), which we consider acceptable. Though such errors could necessitate the use of direct numerical integration for some dynamical problems, they do not significantly affect the statistical nature of the results presented here.

Assumption 4. We neglect resonance phenomena. Since resonances are believed to be a primary mechanism for bringing asteroids to near-Earth space, this omission could be important. To investigate whether resonances dominate the orbital evolution of the S-SEAs, we numerically integrated all 16 asteroids for 1 Myr into the past and future, using the RADAU integrator (Everhart 1985), including perturbations from planets Venus through Neptune (Nolan and Bottke 1995). We monitored close approaches to the Earth as well as secular resonances ν_5, ν_6, ν_{16}, and the Kozai resonances. Our results show that resonances do affect the S-SEAs; we see strong oscillations in both their eccentricities and inclinations. However, in most cases, qualitative changes in the orbits are caused by Earth encounters within a few tens of Earth radii. This property suggests that resonances probably "spread-out" the effective positions of asteroids in a Monte Carlo model, which generally shortens their evolution time scales. However, for the near-Earth asteroid region, the qualitative results of Monte Carlo experiments remain useful.

Our results are supported by Michel *et al.* (1995) and Dones *et al.* (1995), whose numerical integration results show that objects not on "fast-track" resonant orbits (strong and rapid changes in the eccentricity due to resonances) evolve in a "slow-track" fashion (random-walk in semimajor axis due to close approaches to the inner planets), with Earth encounters playing a dominant role. However, their results, along with those of Froeschle *et al.* (1995), confirm that Monte Carlo codes cannot model the complex interactions of secular resonances, mean-motion resonances, and planetary perturbations found for NEAs with $a > 2$ AU.

Recent results by Gladman and Burns (1995) and Dones *et al.* (1995) show that secular resonances are also important for objects on Mars-crossing orbits. Their results show that Monte Carlo codes may overestimate the median evolution lifetime of martian meteorites by nearly an order of magnitude. In some cases, secular resonances may even drive martian meteorites onto Sun-grazing orbits.

Given our model's limitations in regard to resonance dynamics, we follow these guidelines when modeling Earth-crossing objects in the $a > 2$ AU region: (a) No test bodies start in the main belt. (b) The motion of any test body with semimajor axis $a > 2$ AU in our model should be considered part of the slow-track population, even though that fraction of the Earth-crossing asteroid population may be small. However, it is likely that many of the bodies evolving along slow-track dynamical paths make up a large percentage of the observed NEA population. Test bodies on fast-track orbits often reach high eccentricities, placing them in a different portion of (a, e) space than most observed NEAs. Some test bodies even obtain such a high eccentricity that they plunge into the Sun over short time scales (Farinella *et al.* 1994). (c) As we investigate Mars as a possible source for S-SEAs, our results only apply to the fraction of martian ejecta which do not enter secular resonances (i.e., those objects with semimajor axes smaller than Mars' semimajor axis).

II.B. Disruption Frequency

We modified the code of Melosh and Tonks (1993) to account for catastrophic disruption by collisions between asteroids, using the following:

1. The intrinsic collision probabilities and mean impact velocities between a target asteroid (at a given position in (a, e, i) space) and projectiles from both the main-belt and near-Earth asteroid populations (from Bottke *et al.* 1994, 1995).
2. Criteria for disruption as a function of (a) target size, strength, and mass, (b) impactor size and mass, and (c) the relative collision velocity (see below).
3. The number of bodies in the impacting population as a function of size (see below).

To determine (1), we map (in orbital a, e, i space) the collision probabilities and mean impact velocities of test asteroids encountering both the 682 largest main-belt asteroids ($D > 50$ km) (Figs. 2 and 3, respectively) and the 224 known near-Earth asteroids using the method of Bottke *et al.* (1994, 1995) (Figs. 4 and 5, respectively). The 224 NEA orbits are those of the known Apollo, Amor, and Aten asteroids as of January 1993 (from the Minor Planet Center via the database of D. Tholen). The sets of orbits used in these calculations are assumed to be representative of the main-belt and NEA asteroid populations, even though we know that the NEA sample is incomplete and possibly contains strong discovery selection effects (e.g., against Amor-type orbits). By choosing test bodies at regularly spaced intervals in (a, e, i) space and computing the mean collision probability and impact velocities between these test bodies and the impacting populations, we produced a "look-up" map describing collision characteristics everywhere in the terrestrial planet region. Asteroids with orbits between the regularly spaced intervals obtain their collision parameters by interpolation, since both the collision probability and impact velocity maps typically change slowly as a function of position.

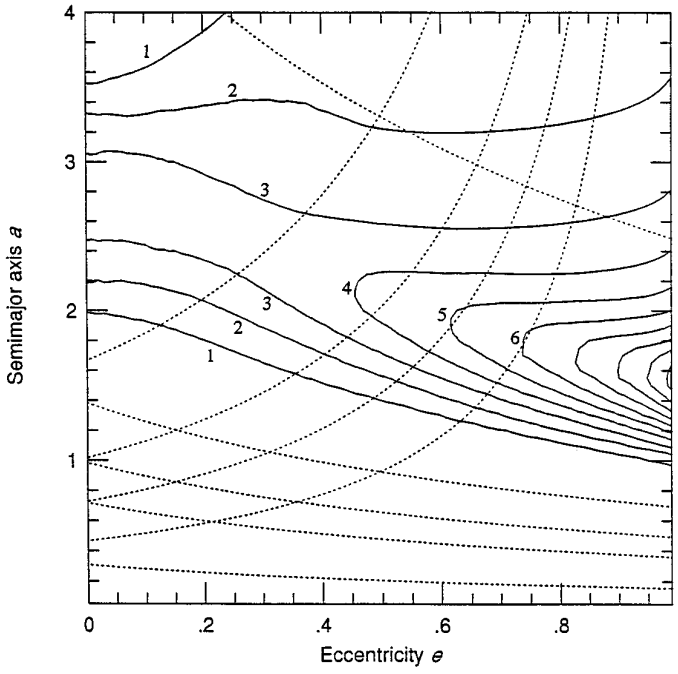

FIG. 2. Map showing the intrinsic collision probabilities for test bodies with an inclination 10° crossing the orbits of 682 main-belt asteroids with $D > 50$ km. Contour spacing is in units of 1×10^{-18} km^{-2} year^{-1}. The dotted lines show where the asteroids have perihelia (q) or aphelia (Q) crossing the orbits of Jupiter or the terrestrial planets (see Fig. 1).

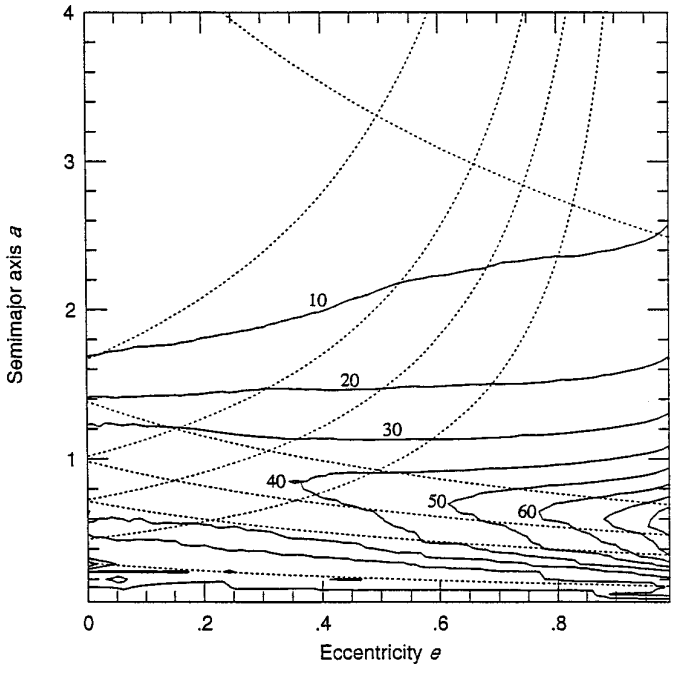

FIG. 4. Map showing the intrinsic collision probabilities for test bodies with an inclination 10° crossing 224 near-Earth asteroids. Contour spacing is in units of 10×10^{-18} km^{-2} year^{-1}. The dotted lines show where the asteroids have perihelia (q) or aphelia (Q) crossing the orbits of Jupiter or the terrestrial planets (see Fig.1).

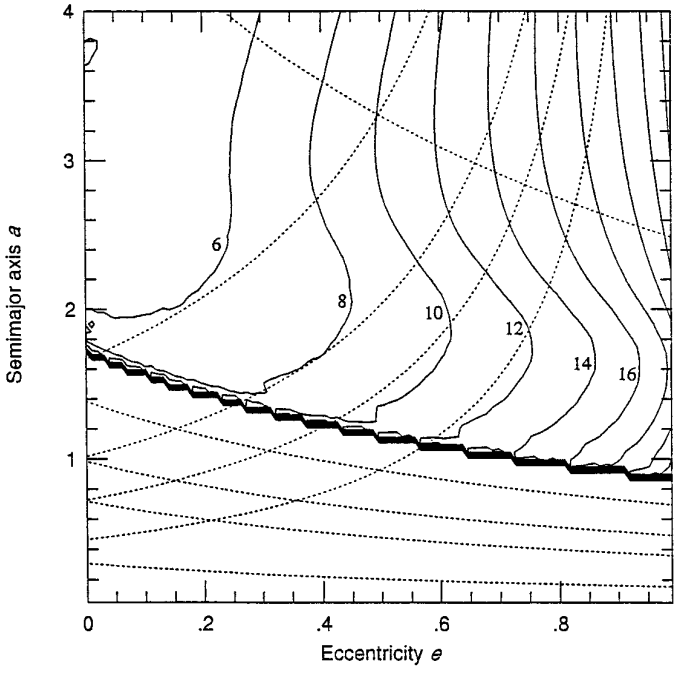

FIG. 3. Map showing the mean impact velocities for test bodies with an inclination 10° crossing the orbits of 682 main-belt asteroids with $D > 50$ km. Contour spacing is in units of 2 km/sec. The dotted lines show where the asteroids have perihelia (q) or aphelia (Q) crossing the orbits of Jupiter or the terrestrial planets (see Fig. 1).

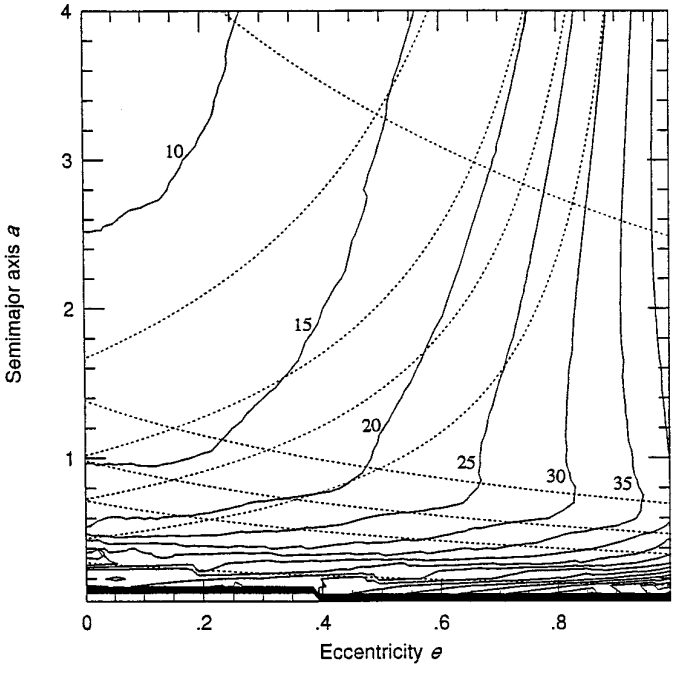

FIG. 5. Map showing the mean impact velocities for test bodies with an inclination 10° crossing the orbits of 224 near-Earth asteroids. Contour spacing is in units of 5 km/sec. The dotted lines show where the asteroids have perihelia (q) or aphelia (Q) crossing the orbits of Jupiter or the terrestrial planets (see Fig. 1).

Once we obtain the collision probabilities and velocities for a given target asteroid, we need to know the size of the projectile required to produce a catastrophic disruption. We define catastrophic disruption as a collision energetic enough to launch half the fragmented target mass away at escape velocity. Since most NEAs are a few km in size or smaller, we assume that asteroid fragmentation will depend on the physical strength of the target body. Thus, we adopt the strength-scaling laws described in Petit and Farinella (1993), which are similar to the results of Housen and Holsapple (1990), to simulate catastrophic disruption of the target body. Their criteria for a barely catastrophic disruption is exceeded if $E_{\mathrm{REL}} > 2SM_{\mathrm{T}}/\rho x_{\mathrm{CR}}$, where ρ is the density of both the impacting and target asteroids (estimated to be 2700 kg/m^3) and M_{T} is the mass of the target asteroid. E_{REL} is the relative kinetic energy of projectile and target asteroids (masses M_{P}, M_{T}, respectively) impacting each other at relative velocity V_{REL}:

$$E_{\mathrm{REL}} = \frac{M_{\mathrm{P}} M_{\mathrm{T}} V_{\mathrm{REL}}^2}{2(M_{\mathrm{P}} + M_{\mathrm{T}})}. \tag{1}$$

S is the minimum specific energy delivered to each body to cause catastrophic disruption, scaled from laboratory impact experiments by the formula

$$S = \left(S_0 + \frac{\pi\gamma}{15} G\rho^2 D^2\right)\left(\frac{D}{0.2\mathrm{m}}\right)^{-1/4}, \tag{2}$$

where $S_0 \approx 3 \times 10^7$ erg/cm^3 for basalt, D is the diameter of the asteroid, and $\gamma = 1$ is a numerical coefficient set by the experimental results. However, since we are dealing with km-sized and smaller asteroids in this model, the self-compression term containing γ is unimportant and can be neglected. Moreover, (2) should be seen as a "best guess" rather than as a quantitatively accurate expression, since S_0 is material dependant and strain-rate scaling does not lead to a satisfactory match between collisional models and the observed size distribution in the main belt (Davis *et al.* 1994). x_{CR} is a numerical coefficient which accounts for non-head-on impacts of the projectile and target body (estimated to be 0.327). By applying the impact velocity computed previously, this criteria allows one to calculate the size of the projectile needed to produce a catastrophic disruption.

Finally, we need to know how many projectiles capable of disrupting a target body exist in either impacting population. We assume a size–frequency distribution for both the main-belt and near-Earth asteroid populations. In the case of the main belt, we assume the size–frequency distribution follows the distribution implicitly suggested by Belton *et al.* (1992), which is extrapolated as a power law (incremental index −2.95) from the small asteroids of the Palomar–Leiden survey (Van Houten *et al.* 1970) and then steepens to an incremental power-law index of −3.5 (Dohnanyi 1969) for asteroids smaller than 175 m in diameter:

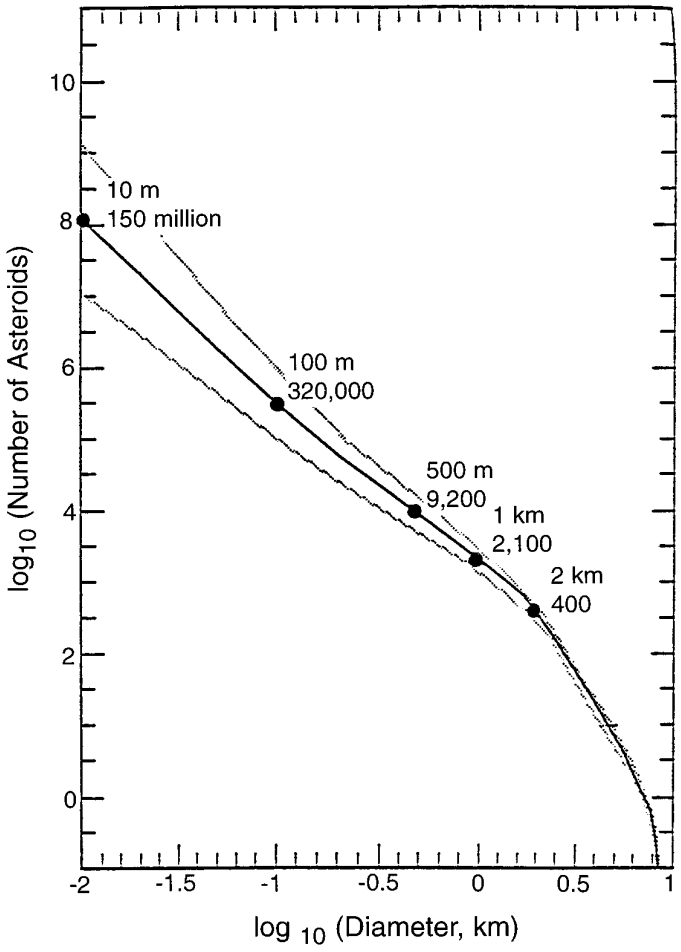

FIG. 6. Estimated number of Earth-crossing asteroids larger than a given diameter (Figure from Morrison 1992).

$$dn = 2.7 \times 10^{12} D^{-2.95} dD \quad \text{for } D > 175\ \mathrm{m} \tag{3}$$

$$dn = 4.7 \times 10^{13} D^{-3.5} dD \quad \text{for } D < 175\ \mathrm{m}. \tag{4}$$

We assume that the NEA population follows the "Spaceguard" size distribution for Earth crossers reported by Morrison (1992) (Fig. 6). The incremental size distribution is estimated to have the following power-law exponents at various size ranges: −3.6 ($D < 0.25$ km), −3.0 ($0.25 < D \leq 2.5$ km), and −4.3 ($D > 2.5$ km). Note that both the main-belt and the NEA population estimates have substantial uncertainties; they should be considered best guesses given our current knowledge.

With this information, we calculate the frequency (events per year) of impacts from these populations into the target body that result in catastrophic disruption of a

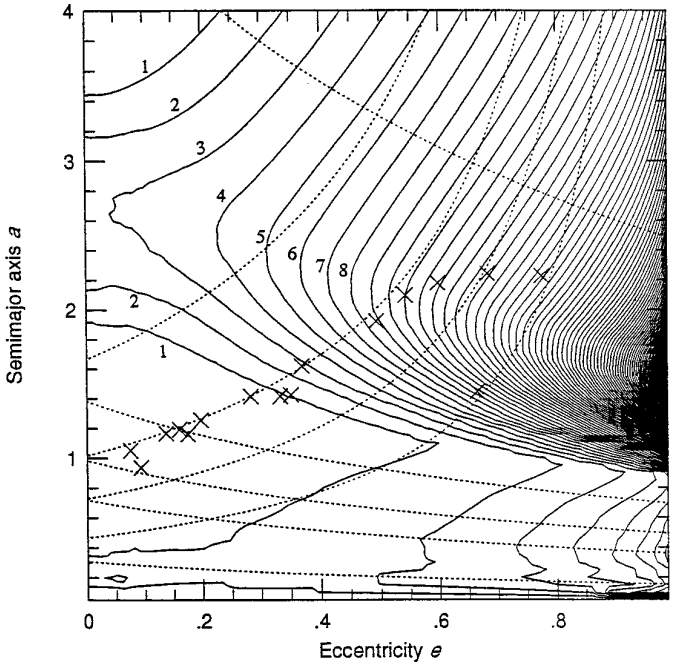

FIG. 7. Map showing frequency of catastrophic disruption based on strength-scaling (Petit and Farinella 1993) for a 100 m target asteroid at an inclination of 10° (Contour spacing is 1×10^{-9} year^{-1}). We see that asteroids with higher eccentricities which cross the main-belt population are much more likely to experience a catastrophic disruption. Asteroids which are collisionally decoupled from the main-belt (e.g., the low-e S-SEAs population) catastrophically disrupt infrequently.

target body. Since NEAs are much less numerous than the main-belt population, catastrophic collisions from NEA projectiles are relatively rare. We then map these results as a function of target size and position in (a, e, i) space. A "slice" of this mapping space at $i = 10°$ is shown in Fig. 7. We find that:

(a) Asteroids with high eccentricities are disrupted more frequently than bodies with low eccentricities, due to high projectile impact velocities and the large amount of time they spend near aphelion among main-belt projectiles. In fact, asteroids exiting the 3:1 or ν_6 resonance into Earth-crossing orbits continue to cross into the main belt, and thus are susceptible to an enhanced likelihood of catastrophic disruption relative to asteroids that remain in the main belt. Qualitatively, this enhanced collision rate may be seen in the orbital distribution of fireballs observed on Earth (Fig. 8). Fireballs are small asteroidal fragments that enter the Earth's atmosphere and are heated to fiery incandescence. In principle, their trajectories can be tracked back into space (e.g., Wetherill and ReVelle 1981, Jopek *et al.* 1995); their orbital parameters suggest that these small fragments may be fresh collisional debris from asteroid impacts on large asteroids. Comparing Fig. 8 with our disruption rate results for test asteroids (Fig. 7) shows that the greatest number of observed fireballs correspond to regions near the $q = 1$ AU line where catastrophic and cratering events (creating small asteroidal fragments) are frequent. However, note that fireball discovery is biased by observation selection effects different from NEA discovery biases.

(b) An asteroid's frequency of disruption drops dramatically when it becomes collisionally decoupled from the main belt (i.e., for aphelion $Q < 1.7$ AU). In fact, the population of observed S-SEAs resides where catastrophic disruptions are infrequent. Again, this paucity of fresh collisional debris can be seen qualitatively in Fig. 8: few observed fireballs come from low-eccentricity orbits.

II.C. Fragmentation Distribution

Our Monte Carlo model also includes fragmentation after a collisional disruption, as modeled by Petit and Farinella (1993). When an asteroid is disrupted (Section II.B), numerous fragments are created, most of which leave the scene of the disruption at velocities greater than escape velocity (by definition of "disruption"). The sizes of the

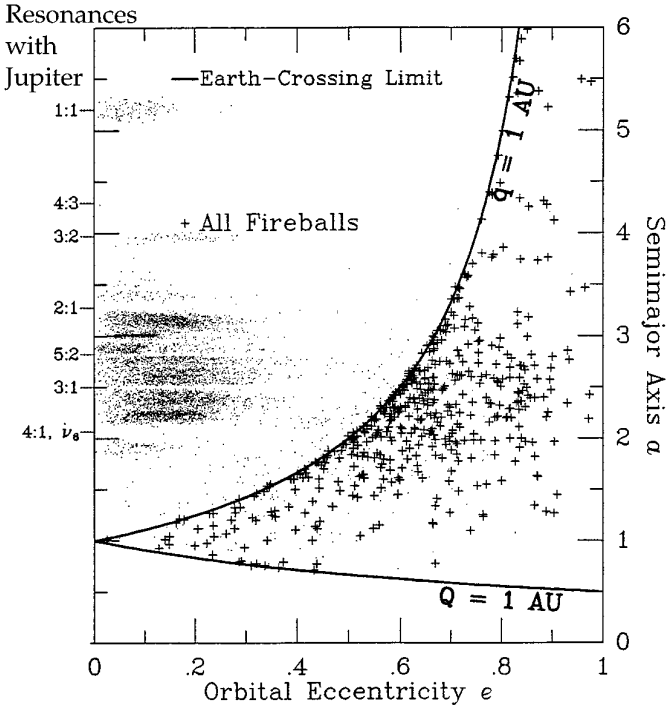

FIG. 8. Plot in (a, e) space showing the positions of the fireballs considered by Wetherill and ReVelle (1981). Note that the highest concentrations of fireballs correlate well with the higher map contours in Fig. 6, which showed the frequency of catastrophic disruptions for a 100 m object. The remaining dots show the orbital positions of the numbered main-belt and all near-Earth asteroids. (Figure from Greenberg and Nolan 1993).

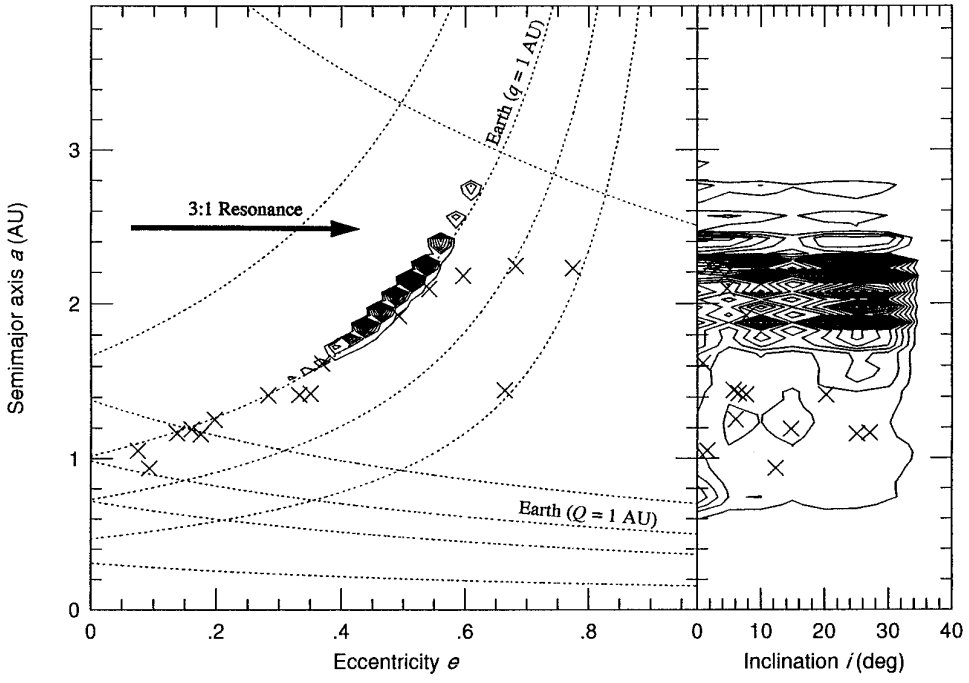

FIG. 9. Contour plot in (a, e) and (a, i) space showing the "relative" residence time of 1 km bodies exiting the 3:1 resonance where they first encounter the Earth (i.e., at $q = 1$ AU). Bodies were started with orbital parameters $a = 2.5$ AU, $e = 0.6$, and $i = 5°, 10°, 15°, 20°, 25°, 30°$. The individual contours show where the asteroids from this source are statistically most likely to spend their time. Thus, high contours show where it is probable to observe objects from a given source. The highest point on this contour plot was given a value of 1000. The contour increment was set at 50 (on this relative scale). In this case, we see that these objects are unlikely to reach the low-e orbits seen for the S-SEAs, making the 3:1 resonance an unlikely source for these objects. Test bodies exiting the ν_6 resonance as they become Earth-crossing yield similar results.

fragments, their relative numbers, and their ejection velocities depend on many factors: the various model parameters, the amount of collision energy partitioned into fragmentation and ejection, and the size, strength, and self-gravity of the target. The mass distribution of the fragments follows the model parameters of Petit and Farinella: $N(>m) = Bm^{-0.5}$ for barely catastrophic collisions, where B is a constant. The exponent is dependant on the impact energy, and is shallower for the more frequent barely shattering impacts than for super-catastrophic collisions.

The fragments themselves are tracked in our Monte Carlo model simulation until they collisionally evolve to be smaller than a pre-selected cutoff size or are dynamically removed from the system. For these runs, we set the cutoff diameter to 50 m for computational expediency; this size is also small enough not to affect our results. Ejection velocities from barely catastrophic disruptions of small km and sub-km sized NEA asteroids are thought to be on order of an asteroid's escape velocity, i.e., ~1 m/sec (Petit and Farinella 1993), so we do not expect that asteroid fragments larger than the cutoff diameter will have significantly different orbits than the original target body. Thus, we give each new fragment that same orbit as the parent body.

II.D. Observation Selection Effects

Observational selection effects from Rabinowitz (1994) are included in our model, allowing us to compare our results directly with their observations of the S-SEAs. Selection effects influence the likelihood of discovering a given size object on a particular orbit, since telescopes can only detect objects within a finite volume of space at specific times during the year. For example, asteroids with orbits that allow them to spend a great deal of time within the search volume (e.g., slow-moving objects or objects that move through the search volume quickly but return frequently) are more likely to be discovered than are other asteroids. Thus, these "special" asteroids will dominate the observed population, making it necessary to account for these biases when we match our dynamical results to the observations.

To compute the severity of these biases in the Spacewatch telescope and search program, Rabinowitz (1993) created a program called the Earth-approacher Simulation Program (ESP) to model the effects of observational bias on an assumed population of Earth-crossing asteroids detected by a simulated telescopic search. By determining which asteroids would be discovered as a function of sev-

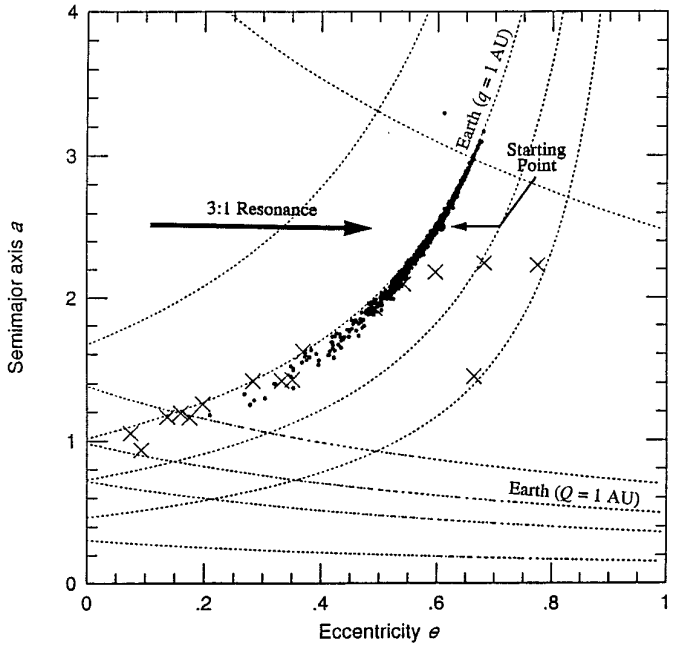

FIG. 10. Plot in (a, e) space showing the evolution of 1 km bodies (and their fragments), with initial orbits of a = 2.5 AU, e = 0.6, and i = 5°, 1 Myr after injection into the system. Most bodies stay close to the q = 1 AU line.

eral detection factors (e.g., limiting magnitude, minimum angular rate, etc.), he computed bias (and inverse ''de-bias'') functions to simulate observational selection effects. To first order, the selection weight is proportional to the ratio of an asteroids' encounter probability with Earth over its encounter velocity with Earth.

The latest results of Rabinowitz (1994) shows a strong bias favoring detection of S-SEAs in low-eccentricity Earth-crossing orbits (with q often between 0.9 and 1.1 AU) and Aten-type orbits for which $a < 1$ AU. Asteroids in these orbits move slowly through the search volume, giving them an enhanced opportunity to be discovered. Small 10–50 m objects with perihelion distances (q) greater than 1.05 AU are considered undetectable. We partially tested his results by assuming the first order relationship above, and calculated our own values for encounter probabilities and velocities (see Bottke and Greenberg 1993). We found comparable results to that of Rabinowitz (1994), including observational selection biases favoring Atens over Apollos (except for asteroids on low-e orbits). The large biases favoring Aten discovery in this discovery-bias model were almost entirely due to high Earth-encounter probabilities; encounter velocities change too slowly over the Aten/Apollo region to contribute substantially to the Aten biases.

The extremely strong bias favoring discovery of objects in Aten-type orbits has been questioned by G. B. Valsecchi (personal communications), who claims that Rabinowitz's approach may not account for more subtle observational selection effects. In fact, a preliminary reexamination and recalculation of Spacewatch's observation selection effects by R. Jedicke (personal communication) suggests that Atens may not be so heavily biased toward detection and higher inclination S-SEA-type objects may be easier to detect. Future studies of observational selection effects based on the Spacewatch search program may yield additional constraints for near-Earth asteroids. Thus, though our results are based on the best bias functions currently available, they will be subject to revision if Spacewatch bias functions are modified.

II.E. Experimental Procedure

We inject all test particles from given starting points at the same time rather than as a steady-state production, assuming that both models are equivalent for our purposes of determining evolutionary paths. (i.e., bodies injected into the ''same-time start'' model create a ''road-map'' showing their most probable evolutionary paths; bodies injected into the steady-state model follow the same road-map, leading to identical results). We let those bodies (and their fragments) dynamically and collisionally evolve until they hit a terrestrial planet, collisionally evolve below the cutoff diameter of 50 m, or are ejected out of the system, most often by Jupiter. (The near-Earth asteroid dynamical paths are described in detail in Appendix A).

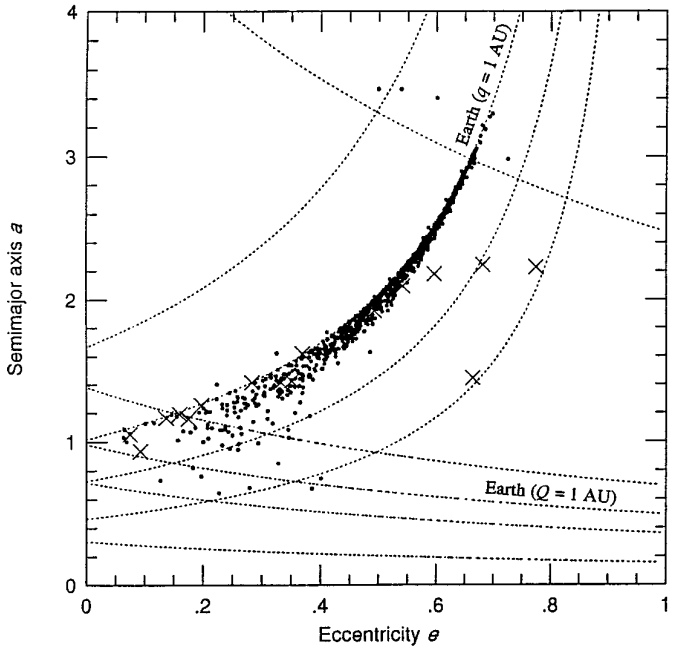

FIG. 11. Plot in (a, e) space showing the evolution of 1 km bodies (and their fragments), with initial orbits of a = 2.5 AU, e = 0.6, and i = 5°, 5 Myr after injection into the system. A few bodies have reached the low-e region consistent with the S-SEA population given by Rabinowitz *et al.* (1993).

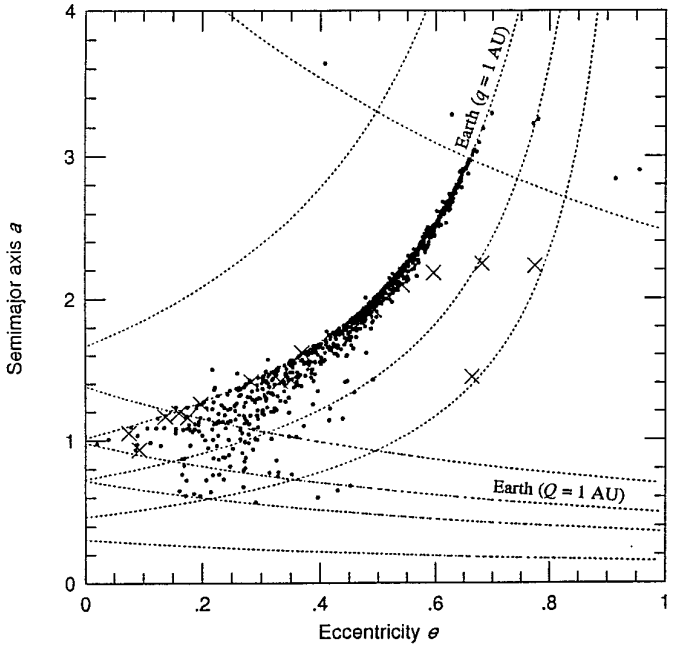

FIG. 12. Plot in (a, e) space showing the evolution of 1 km bodies (and their fragments), with initial orbits of a = 2.5 AU, e = 0.6, and i = 5°, 10 Myr after injection into the system. The distribution of particles reaching low-e orbits have begun to spread along Venus and Earth-crossing orbits.

To track the evolutionary paths of the test bodies, we record the total amount of time spent in each bin of (a, e, i) space by each asteroid. The bins with the most recorded time, modified by observational selection effects, correspond to the most likely location for detection. We display this information using contour plots which show the residence time of these bodies in (a, e) and (a, i) space (Fig. 9). The contours show where the asteroids (and their fragments) from a given source are statistically most likely to spend their time and thus where they are most likely to be observed. A high contour may correspond to one body spending a great deal of time in a particular region or 100 bodies spending relatively little time there.

III. RESULTS

III.A. Fragments from the Main Belt

One likely source for the S-SEAs is collisional debris exiting the 3:1 or ν_6 resonances once they become Earth crossing (at q = 1 AU) (Wetherill 1985, 1988). To test this hypothesis, we examine the orbital evolution of test bodies (D = 1 km) with initial orbits of a = 2.5 AU, e = 0.6, and i = 5°, 10°, 15°, 20°, 25°, 30° (for the 3:1 resonance) (Fig. 9) and a = 2.1 AU, e = 0.524, and i = 5°, 10°, 15°, 20°, 25°, 30° (for the ν_6 resonance) (results similar to Fig. 9). We purposely chose large bodies so we could determine the effects of comminution on dynamically evolving main-belt fragments.

Fig. 9 (a, e) shows that main-belt objects, starting from either of the 3:1 or ν_6 resonances transport orbits, are unlikely to dynamically evolve into S-SEAs. Objects from these sources frequently disrupt, impact the Earth, or are ejected from the system before reaching the low-e orbits ($e < 0.2$–0.3) seen among the S-SEAs. The highest contours correspond to bodies that have achieved Amor-like orbits (i.e., orbits which are not Earth-crossing but Mars-crossing), where dynamical spreading times are longer. As such, they show high residence times in high-e orbits along the q = 1 AU line where collisions are frequent, and no signature in low-e orbits along the same line, even though observational biases favor detection in that region. Furthermore, though frequent impacts with the main belt would produce fresh collisional debris, there is no reason for this debris to create the clear excess of small bodies seen in low-e as S-SEAs. If these sources are responsible for the S-SEAs, we should see a hierarchy of debris stretching from the source to the S-SEA orbits and a steep power-law size–frequency distribution for the entire population, which is not observed.

If we look at (a, i) space, we find similar results to those seen in (a, e) space, though we do find that bodies with high inclinations are just as likely to be observed as bodies

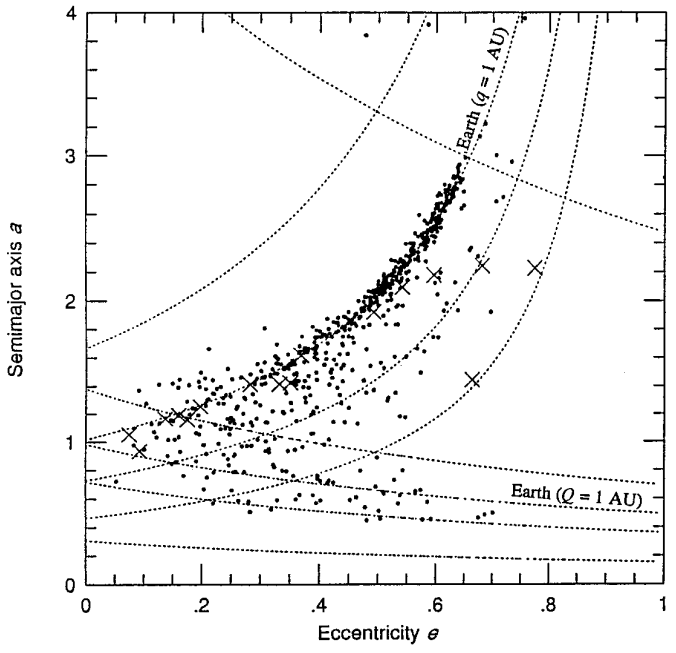

FIG. 13. Plot in (a, e) space showing the evolution of 1 km bodies (and their fragments), with initial orbits of a = 2.5 AU, e = 0.6, and i = 5°, 50 Myr after injection into the system. The distribution of particles is now spread widely over the terrestrial planet region, though many fragments are still concentrated in regions where asteroid disruption rates are high.

with low inclinations below $a < 1.4$ AU. This result is surprising, given that the observational selection effects of Rabinowitz (1994) strongly favor the detection of asteroids at low inclinations. However, high contours seen between inclinations of 20°–30° at $a > 1.4$ AU allow us to infer that ejecta evolving out of the 3 : 1 resonance on high inclination orbits are less susceptible to planetary perturbations and asteroid collisions, making them less likely to spread (in inclination space) or be removed from the system than ejecta on low-inclination orbits.

It is important to emphasize that the relative residence time contour plots presented in this paper show where asteroids are most likely to be observed if they start from a given source, which can be very different from results showing the complete evolutionary paths followed by those asteroids due to collisions and observational biases. For example, Figs. 10–13 show the (a, e) positions of 1 km test bodies (and their comminution fragments) at various times after their initial injection into an orbit of $a = 2.5$ AU, $e = 0.6$, and $i = 5°$ (i.e., the same run shown in Fig. 9 with only a single choice of inclination). For this run, we started with only 1000 test bodies, though disruption events, fragmentation, ejection events, and planetary impacts modify this number. No observational biases are used. The results of this run indicate that a few test bodies reach orbits consistent with S-SEA orbits (i.e., the low-e range) after a few million years of evolution, which would appear to contradict the results of Fig. 9. However, only a small fraction (< 1%) of the objects make it to that region, and even fewer spend any significant time there; many more objects stay at higher-e, where they persist long after initial injection. Furthermore, fragmentation events create many new objects in that region. Figure 14 shows the residence time contour plot for this run, though this time no observational biases are included. It verifies that most test bodies spend their time in high-e orbits. If we compare these results to Fig. 9, which used more bodies, higher inclination orbits, and included observational selection effects, we find little difference.

Objects started with deeper Earth-crossing orbits (i.e., $e = 0.65, 0.70$) do not dynamically evolve into low-e orbits. For example, Fig. 15 shows a test case where we started many 1 km test bodies with initial orbits $a = 2.5$ AU, $e = 0.65$, and $i = 5°, 10°, 15°, 20°, 25°, 30°$. These objects evolve into orbits which are consistent with some of the higher-eccentricity S-SEAs and can evolve (with time) into orbits consistent with Aten asteroids (i.e., asteroids having semi-major axes (a) smaller than 1 AU and aphelion distances (Q) greater than 0.983 AU). Neither evolution path is close to the observed distribution of low-e S-SEAs. The paths most often followed by these objects, as shown by their high residence time contours, correspond well with the dynamical paths described in Appendix A (i.e., objects started on these types of orbits follow contours of Tisserand invariant, allowing them to transition into Aten orbits more readily than the previously run). Thus, Aten asteroid production may require that we start with asteroids on shallow or moderate Earth-crossing orbits rather than barely Earth-crossing orbits.

In summary, if the main belt is the primary source for the S-SEAs, one must explain why the Spacewatch telescope isn't finding large numbers of small asteroids with high-e orbits; they should be visible in large numbers if they exist. In addition, we should expect to see by-products of asteroid comminution all along the $q = 1$ AU line.

III.B. Ejecta from Mars

Another possible source for the S-SEAs is small-body ejecta from Mars. To test Mars as a source, we start with 100,000 bodies with an ejecta velocity distribution with the cumulative mass fraction ejected at speeds proportional to $V^{-9/4}$ (see Farinella *et al.* 1993 for details) and a random direction. This ejecta velocity distribution "at infinity" (i.e., once the ejecta clears the gravitational well of Mars) peaks near 2.8 km/sec. These bodies are chosen to be 100 m in diameter, an order of magnitude smaller than the main-belt case, since it is likely that even large planetary ejecta fragments are much smaller in size and number than NEAs derived from the main belt. These sizes are somewhat arbitrary, but they do allow a meaningful comparison between different asteroid sources with different evolutionary paths and comminution rates. These small ejecta are comminuted below the Spacewatch detection limit more quickly than larger asteroids evolving from the main belt. Recall, however, that important secular resonances in this region are not modeled by our code; our results only apply to those bodies not entering resonances (see Section II.A).

Our results show that the highest model density contours for Mars ejecta near the $q = 1$ AU line correlate fairly well with the actual orbits of the S-SEAs with eccentricities from 0.1 to 0.3 (Fig. 16) in (a, e) space. These contours also predict an observable martian ejecta component among S-SEAs with larger eccentricities. However, the flux of fragments from the 3 : 1 or ν_6 resonances is large enough at high eccentricities (>0.35–0.4) (Fig. 9) that such S-SEAs are more likely to be derived from the latter source. Asteroids dynamically evolve very slowly near Mars, due to Mars' weak gravitational field (relative to Earth). If the ejecta are launched at low velocities (below the velocity distribution peak "at infinity" of 2.8 km/sec), we find that most ejecta take a long time (usually 10–100 Myr, and sometimes longer) to reach Earth-crossing orbits, similar to results found by Vickery and Melosh (1993) and Wetherill (1984). However, we note that high velocity ejecta can reach Earth-crossing orbits quickly if its initial launch orientation is in the appropriate direction. However, the fraction of ejected mass traveling at these higher velocities is

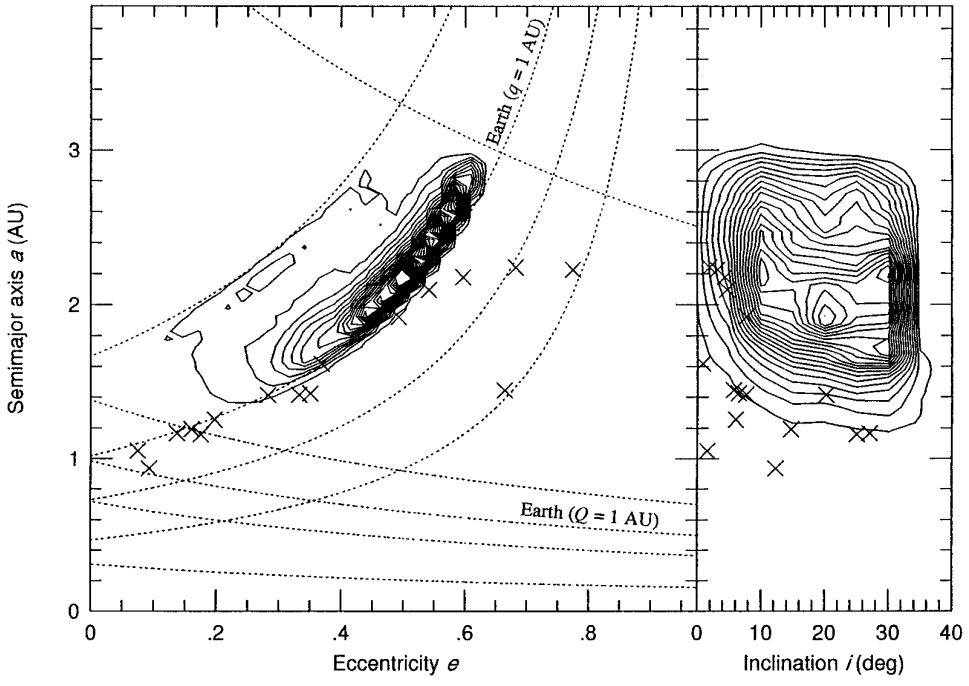

FIG. 14. Contour plot in (a, e) and (a, i) space showing the "relative" residence time of 1 km bodies with initial orbits of a = 2.5 AU, e = 0.6, and i = 5°, 10°, 15°, 20°, 25°, 30° (for the same runs shown in Fig. 9). No observational biases are included. The highest point on this contour plot was given a value of 1000. The contour increment was set at 50 (on this relative scale). A comparison between this plot and Fig. 9 shows some differences in (a, e) and (a, i) space, since we can now "see" beyond the q = 1.05 AU line.

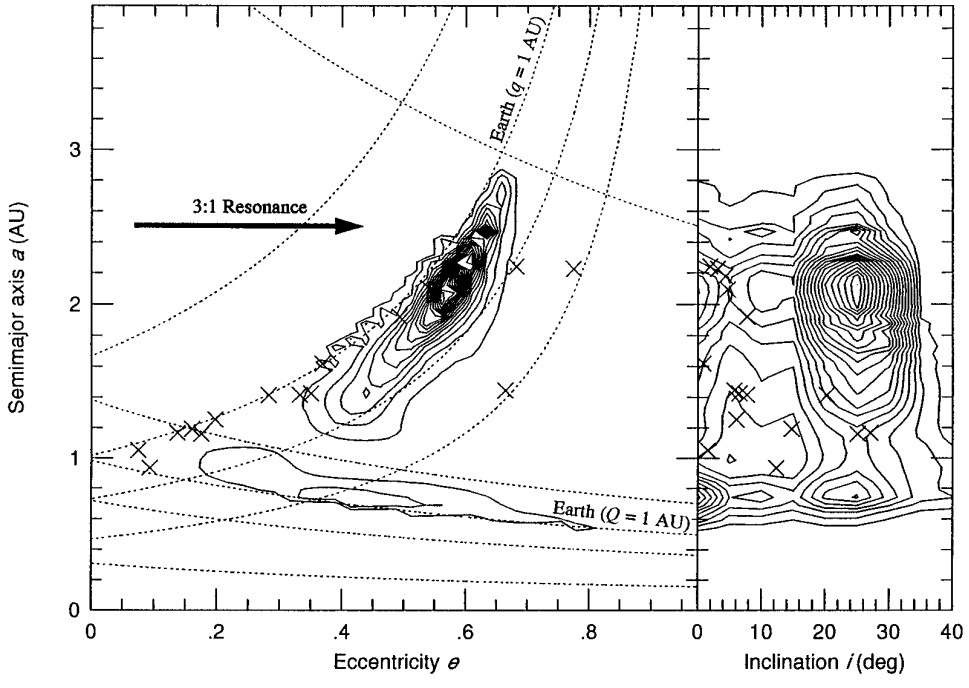

FIG. 15. Contour plot in (a, e) and (a, i) space showing the "relative" residence time of 1 km bodies with initial orbits of a = 2.5 AU, e = 0.65, and i = 5°, 10°, 15°, 20°, 25°, 30°. The highest point on this contour plot was given a value of 1000. The contour increment was set at 50 (on this relative scale). We see that these astroids do not evolve into the low-e S-SEA orbits either, although they can evolve into orbits consistent with Aten asteroids. Note the high contours at inclinations between 20° and 30°. Planetary perturbations are less likely to spread objects with high inclinations in inclination space.

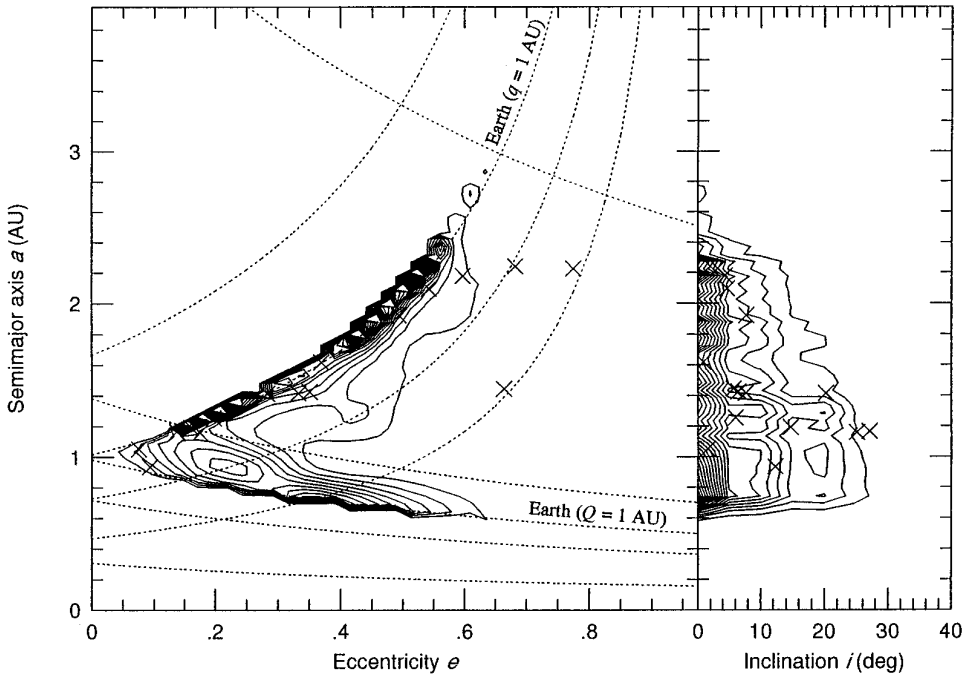

FIG. 16. Contour plot in (a, e) and (a, i) space showing the "relative" residence time of ejecta starting from Mars. The initial ejecta fragments (D = 100 m) are given a random ejection trajectory and a velocity chosen by a Gault-type ejecta velocity distribution, with the cumulative mass fraction ejected at speeds proportional to $V^{9/4}$. The highest point on this contour plot was given a value of 1000. The contour increment was set at 50 (on this relative scale). Mars ejecta evolves into (a, e) positions consistent with the low-e orbits necessary to produce the observed S-SEAs. However, residence time contours shown at high inclinations are relatively low, inconsistent with low-e S-SEA orbits with $i > 20°$.

likely to be low, unless Mars ejection velocities are higher than expected (Wetherill 1984, Farinella *et al*. 1993). Low-velocity ejecta spend a great deal of time just beyond the q = 1 AU line, between $e \sim 0.15$ and 0.27, yielding high residence time contours. Once these ejecta reach the q = 1 AU line, they spread out quickly, creating low level residence time contours extending out beside the Q = 1 AU line. We see no S-SEAs along the Q = 1 AU line at eccentricities > 0.1, consistent with the low model contours in this region, though high observational selection effects for Aten-type orbits qualify this match (this effect is discussed in more detail in the next section).

We find that Mars' residence time contours in (a, i) space are not consistent with all of the S-SEAs. The highest contour levels fit best with the low and moderate inclination S-SEAs, though the model shows a few high-inclination S-SEAs. These results stem from two factors: (a) only a small fraction of all Mars ejecta achieve high inclinations as it dynamically evolves, and (b) Rabinowitz's (1994) observational selection effects for the S-SEAs are heavily weighted toward detection at low inclinations, making detection at high inclination more difficult. Consequently, though Mars' ejecta fits some of the S-SEA orbits, they cannot be the sole source for the S-SEAs at low eccentricities. Note that secular resonances, which may be important for Mars ejecta, can increase inclination more effectively than the planetary perturbations considered in our model (Gladman and Burns 1995).

Mars ejecta evolution is more explicitly shown in Figs. 17–20, where we plot the (a, e) positions of the test bodies (and their comminution fragments) at various times after their ejection from Mars. For this run, we started with only 1000 test bodies, though disruption events, fragmentation, ejection events, and planetary impacts modify this number. Their initial orbits correspond to a random trajectory and a velocity of 1 km/sec once they had cleared the gravitational well of Mars (i.e., V_∞ = 1 km/sec). We choose this low velocity to simulate the evolution of a large fraction of the ejecta. No observational corrections were applied here, which allows one to examine the collisional and dynamical evolution of ejecta well beyond the range of detectability from Earth. This run shows that most ejecta stay far from the q = 1 AU line and evolves slowly.

It should be mentioned that the collisional evolution of Mars-crossing asteroids in this model does not include effects of impacts by asteroids in the poorly known population beyond $q > 1.3$ AU crossing Mars' orbit (i.e., beyond the Amor near-Earth asteroid population). However, increasing the disruption frequency of asteroids in this region would not affect the results presented here, because more disruptions would, at best, only slightly enhance the total population of small ejecta fragments far from the q = 1

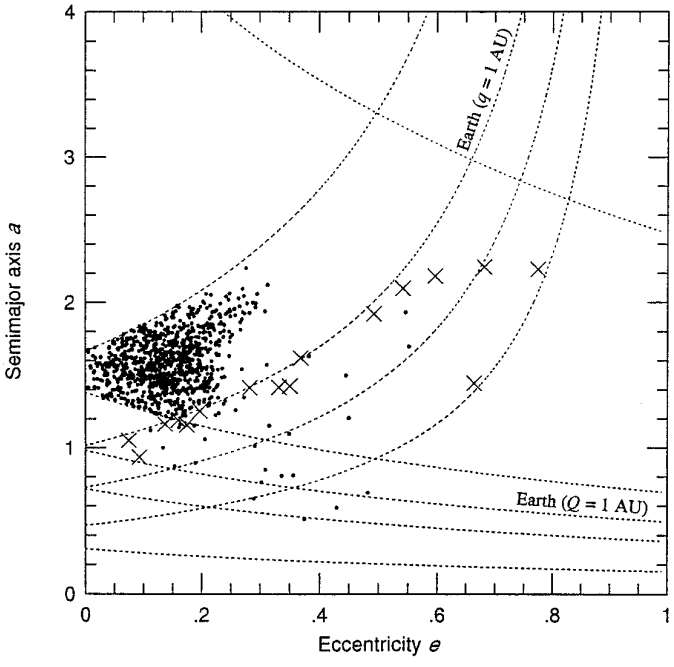

FIG. 17. Plot in (a, e) space showing the evolution of 1000 100-m bodies 20 Myr after they were ejected from Mars with a random trajectory and an initial velocity of $V_\infty = 1$ km/sec. Some bodies have been removed by planetary impact, catastrophic disruption, or ejection. Comminution fragments larger than the cutoff diameter of 50 m are shown.

AU line. Thus, this change would effectively only increase the size of our starting population, keeping the relative contour levels the same as before.

III.C. Stochastic Breakup of Amor Asteroids

Mars ejecta are not the only bodies occupying Mars-crossing orbits beyond the reach of the Earth at $q > 1$ AU. Amor asteroids, which presumably evolved from main-belt chaotic zones through the complex interactions between Mars perturbations, mean-motion resonances, and secular resonances, are also found in this region. The Amor population is not well characterized, since most are too small and too far away to be seen from Earth. However, some km-sized bodies have been observed at low eccentricities, implying that more exist at smaller sizes.

Some of these bodies might be dynamically indistinguishable from Mars ejecta (P. Farinella, personal communication), and would evolve toward Earth-crossing orbits in a similar way. In fact, many Amors are already on high inclination orbits similar to those found among 4 of the 16 S-SEAs. Thus, these orbits could potentially match S-SEA dynamical constraints better than Mars ejecta.

To test this idea, we started several 200 m objects with initial orbits $a = 1.4$ AU, $e = 0.1$, and 0.2, and $i = 5°$, 10°, 15°, 20°, 25°, 30° (Fig. 21). We let them collisionally and dynamically evolve according to our procedure described previously. As expected, we found that Amors evolve in similar ways to that of Mars-ejecta; Mars-crossing fragments often evolve slowly toward Earth-crossing orbits, allowing disruption events to create many small fragments. Eventually, these fragments reach Earth-crossing orbits, where they are quickly spread along the $q = 1$ AU line. We find that the (a, e) residence time contours look very similar to Mars ejecta (Fig. 16), but that the (a, i) contours are much higher at high inclinations.

Thus, Amor asteroids provide a good fit to the data, though again we caution that secular resonances may make S-SEA inclination constraints irrelevant. We note that since Amor asteroids originally come from the main belt, it would be worth examining how their dynamical paths allow them to reach low-a, low-e orbits. However, we leave this issue to more advanced models which can account for resonance phenomena, since resonances are likely to play a substantial role in this region of space.

III.D. Ejecta from the Earth–Moon System or from Venus

Next, we consider planetary ejecta from either the Earth–Moon system or Venus producing the S-SEA population. As in the martian test case, we start with 100,000 100-m diameter bodies which were given a random trajectory and an ejecta velocity distribution similar to that described in Section III.B. The ejecta velocity distribution "at infinity" that we use varies with the choice of planet, since each planet's escape velocity is different. For exam-

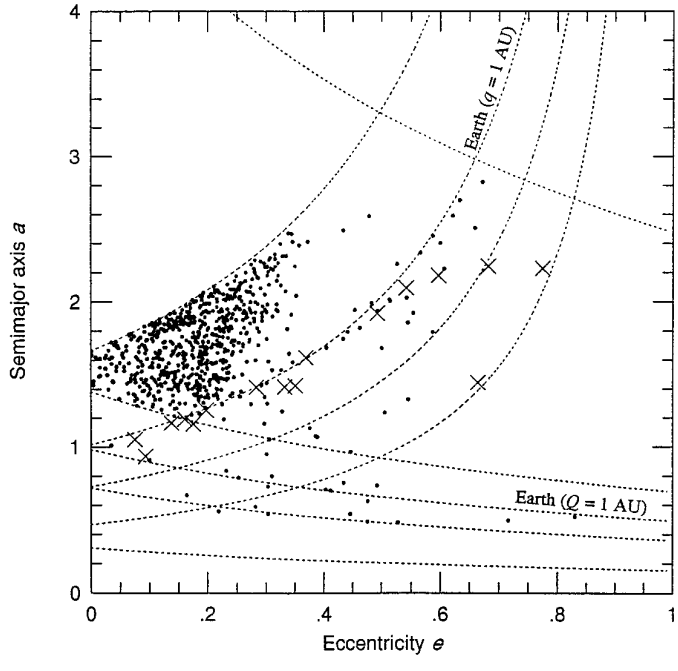

FIG. 18. Same as Fig. 17, 100 Myr after Mars ejection.

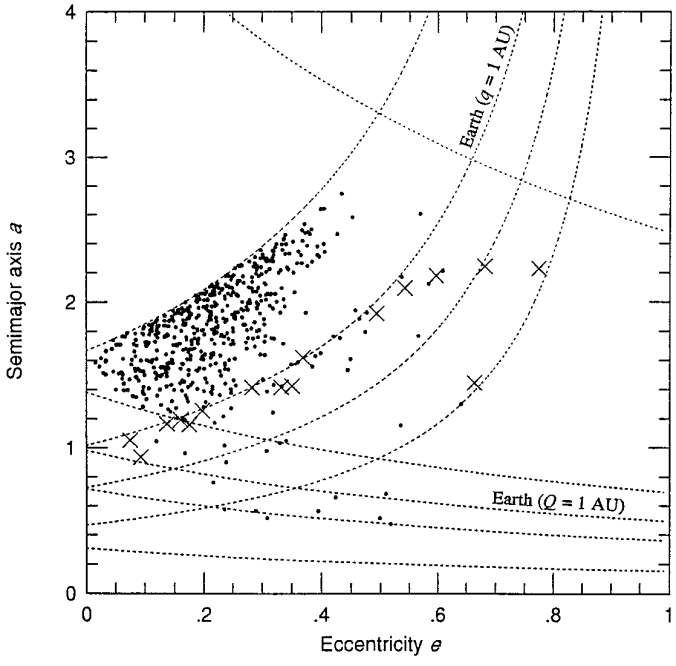

FIG. 19. Same as Fig. 17, 200 Myr after Mars ejection.

ple, the peak of the velocity distribution for Earth is ~6 km/sec, while the peak for the Moon is only 1.3 km/sec (Farinella *et al.* 1993, Eq. (3)). Thus, even though ejecta from the Moon, with its lower gravitational acceleration, would more readily achieve escape velocity, we find that Earth ejecta would more readily achieve high inclination orbits similar to those among the low-e S-SEAs. However, the lifetime of asteroid fragments on low-e Earth-crossing orbits is short enough (~10–20 Myr) that it is unlikely that a large asteroid has impacted Earth or Venus during that time, probably ruling them out as a potential S-SEA source (see Section IV.A for more detail). Thus, our examination will focus on the Moon as a source for the S-SEAs, though we have tested ejecta launched from all three sources.

As with the other cases, we tracked the evolutionary paths of planetary ejecta until they exited the system or collisionally eroded below our cutoff diameter of 50 m. The relative residence time for these particles is shown in Fig. 22 for material ejected from the Moon. Results are nearly identical if the Earth or Venus is the source, though the inclination distribution for their ejecta is higher.

High contours in (a, e) space, shown in Fig. 22, lie all along the $q = 1$ AU and $Q = 1$ AU lines. Several of these high contours correlate with the positions of S-SEAs with $e < 0.2$. Ejecta residing in these low-e orbits are collisionally decoupled from the main belt, allowing them to survive and maintain their steep size–frequency distribution. However, the dynamical lifetimes of objects in this region are only ~10–20 Myr, such that S-SEAs from this source would have had to have been produced in a recent impact event. The match between S-SEAs and high residence time contours at larger eccentricities ($e > 0.2$) is less satisfying, but it is probable that these S-SEAs are main-belt fragments exiting the 3:1 and ν_6 resonances. Thus, detection of lunar ejecta in this region is unlikely, since main-belt fragments dominate the local asteroid population. An even poorer match is found along the $Q = 1$ AU line (all the way to $e \sim 0.6$) where few objects are actually observed. High contour values in this region are primarily due to the bias correction factors of Rabinowitz (1994). In comparison, the residence time contours for Amor asteroids over the same region are much lower.

The residence time contours in (a, i) space also show a poor fit to the data (Fig. 22). Lunar ejecta does not readily achieve high inclinations; contours of constant Tisserand invariant at different inclinations show that Earth perturbations only have a limited effect in increasing inclinations (Nolan 1994). Thus, at best, lunar ejecta provides a good fit for only the low-i S-SEAs. Ejecta fragments from the Earth or Venus are a somewhat better fit to more moderate-i S-SEAs, since high ejecta velocities are needed to launch material to planetary escape velocities, but the overall fit to S-SEA dynamical constraints remains poor.

Only three Atens (objects between $a = 1$ AU and $Q = 1$ AU) have been found since Spacewatch started operation in 1990 (Jim Scotti, personal communication). The relative paucity of Aten discoveries does not fit the model distribution in Fig. 22. It is possible that our model fails to account for some mechanism which either removes Atens or keeps other asteroids from evolving into Atens. Here we list a

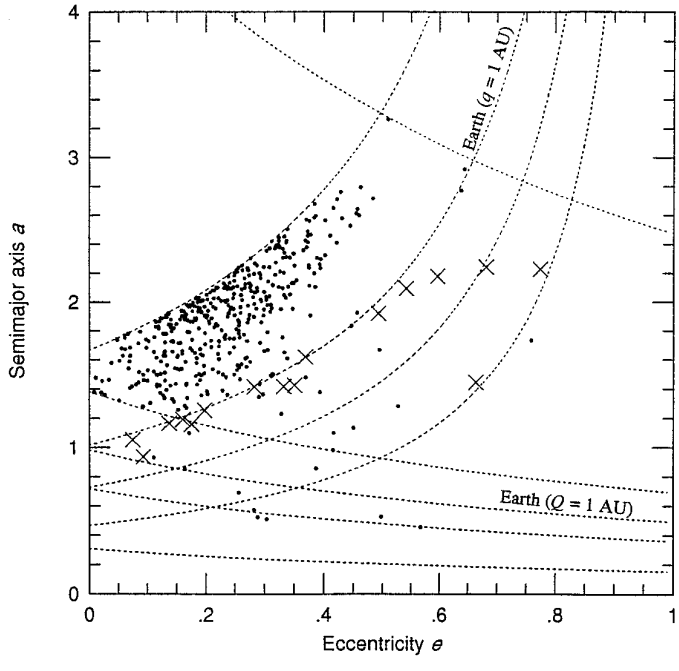

FIG. 20. Same as Fig. 17, 300 Myr after Mars ejection.

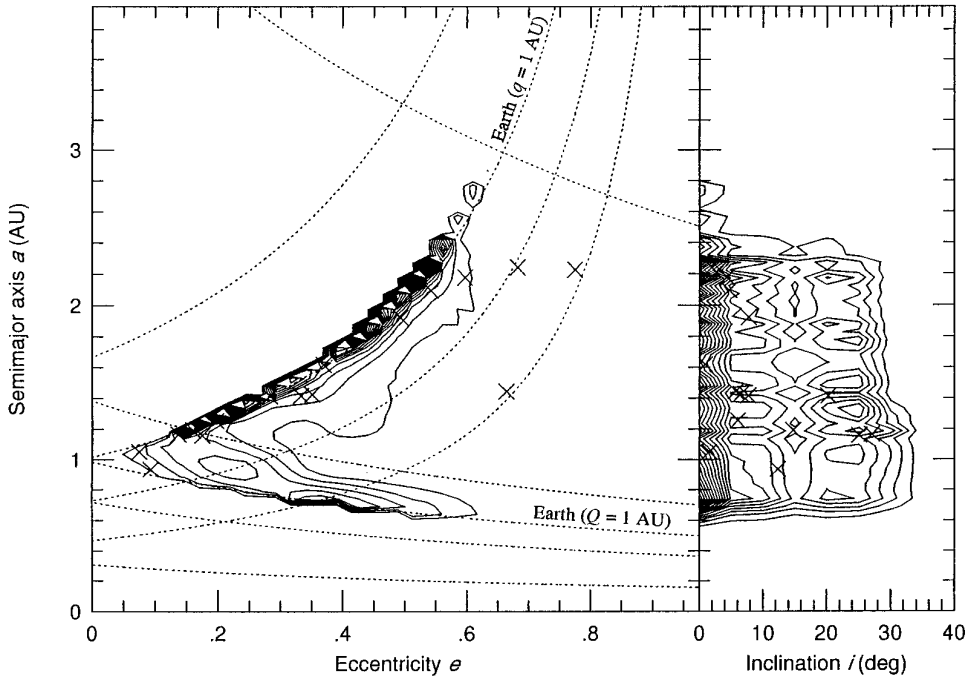

FIG. 21. Contour plot in (a, e) and (a, i) space showing the "relative" residence time of 200 m bodies with initial orbits of a = 1.4AU, e = 0.1 and 0.2, and i = 5°, 10°, 15°, 20°, 25°, 30°. No observational biases are included. The highest point on this contour plot was given a value of 1000. The contour increment was set at 50 (on this relative scale). We find that Amor asteroids and their fragments follow evolutionary paths similar to Mars ejecta, though the Amor's residence time contours in (a, i) space provide a better fit with the low-e, high-i S-SEAs.

few possibilities, all of which will require further study beyond the scope of this paper:

(a) Small asteroids may be removed from or be prevented from reaching Aten orbits by resonance phenomena: It is possible that resonances prevent S-SEAs from following the dynamical paths used by our Monte Carlo model or they might help trap S-SEAs in their current orbits when they enter low-e orbits. Conversely, Earth resonances may scatter Aten asteroids on short time scales.

(b) A second possible mechanism for removing small Atens is the thermal drag force (Rubincam 1994). This variant of the Yarkovsky effect, which is not dependent on rotation direction, may cause small bodies (up to tens of meters in diameter) to be dragged toward the Sun as they absorb sunlight over the visible wavelengths and reradiate that energy over the infrared wavelengths in the direction opposite orbital motion. Since thermal drag forces become more effective near the Sun, this mechanism could preferentially pull small Aten asteroids into the Sun or into close encounters with planets while having a negligible effect on most Apollos and Amors. However, little quantitative research has been done on this mechanism; more work is needed to understand the relative importance of this effect when compared to planetary close encounters.

(c) Observational selection effects: The observational selection effects computed for the Aten region may be too high, i.e., detection of Aten asteroids may be more difficult than concluded by Rabinowitz (see Section II.D).

III.E. Stochastic Breakup of a Near-Earth Asteroid

Finally, we consider the possibility that a stochastic breakup of a NEA in a low-e orbit could produce the observed population of S-SEAs. We find that test asteroids started in regions near the current positions of the S-SEAs can match their (a, e) orbital positions. However, the inclinations of fragments from a single parent body remain correlated with the inclination of that parent body. Observations of the S-SEAs show that their inclinations are well distributed between 0° and ~30°, similar to the inclination of asteroids from the main belt. Furthermore, multiple catastrophic disruptions in this region of space are extremely unlikely, given the short "clearing-time" (10–20 Myr) caused by Earth (and Venus) perturbations. As a result, this region of space is unlike the Amor asteroid region described in Section III.C. We conclude that a single catastrophic disruption of a NEA cannot produce the observed population, and that the multiple disruption events at low-e over short time scales are unlikely.

IV. DISCUSSION

Our calculations of the distribution of planetary ejecta provide a marginal-to-poor fit to the population of small

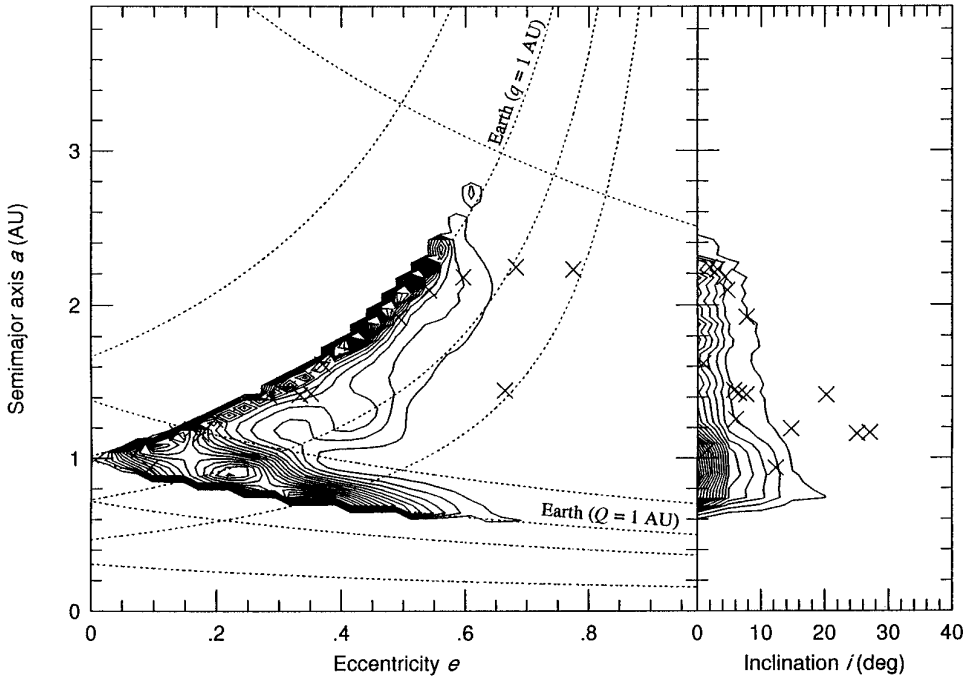

FIG. 22. Contour plot in (a, e) and (a, i) space showing the "relative" residence time of ejecta starting from the Moon. The initial ejecta fragments (D = 100 m) are given a random ejection trajectory and a velocity chosen by a Gault-type ejecta velocity distribution, with the cumulative mass fraction ejected at speeds proportional to $V^{-9/4}$. The highest point on this contour plot was given a value of 1000. The contour increment was set to 50. Note that, similar to Mars ejecta, the higher contours correlate well with the positions of the low-e S-SEAs. However, Lunar ejecta show high residence time contours along the Q = 1 AU line, inconsistent with the observed S-SEA orbits. Moreover, few residence time contours reach high inclinations. Test bodies starting from the Earth and Venus give similar results, though higher ejection velocities yield ejecta with higher inclinations.

Earth-approaching asteroids observed by Spacewatch. Thus, some of those S-SEAs could be from the Earth, Moon, Venus, or Mars, but not enough to define a population. Mars-crossers and Amors are more effective sources. By comparing our results to other lines of evidence regarding planetary ejecta, specifically (a) the ejecta process itself and (b) evidence from planetary meteorites, we hope to determine whether any of these sources are even partially viable or whether they can be dismissed entirely.

IV.A. Ejection of S-SEAs from Planets

The assumption that planetary ejecta can form a fraction of the observed S-SEAs implies that a large cratering event (or events) must have occurred on the Earth, Moon, or Venus within the dynamical lifetime of the S-SEAs (~10–20 Myr) or that fragments from a older martian cratering event ~200 Myr ago are gradually evolving into Earth-crossing orbits. These dynamical lifetimes place additional constraints on the potential source regions; we can use them to check how often asteroids large enough to eject 10–50 m fragments impact the terrestrial planets.

In the former case, we estimate that the largest impactor likely to have hit the Moon in that time would be a $D \sim$ 1 km asteroid, while a $D \sim 3$ km asteroid should hit Earth or Venus within that same time on average (Bottke *et al.* 1995). However, it is not known what size crater and impact parameters would be sufficient to eject 10–50 m objects from any of the terrestrial planets. The escape velocity of the Moon (V_{ESC} = 2.4 km/sec) is significantly lower than that of either the Earth (V_{ESC} = 11.2 km/sec) or Venus (V_{ESC} = 10.2 km/sec), which could enhance that body's ability to eject fragments.

In the Mars ejecta case, these model constraints are more relaxed. Vickery and Melosh (1987) estimated that a crater larger than 100 km in diameter formed roughly 200 Myr ago could have launched the parent bodies of the SNC meteorites. Ejecta from that impact event would evolve toward Earth-crossing orbits slowly and be comminuted along the way. The longer evolution time and decreased delivery efficiency (i.e., relative to the Earth, Moon, and Venus) of Mars ejecta is compensated somewhat by the expected large mass flux of ejected material from such a large impact.

How much non-shocked material is ejected at escape velocity from cratering events on the terrestrial planets? To find out, we extrapolated the size–velocity ejecta distri-

butions of Vickery (1986, 1987) to planetary escape velocities. Vickery measured the sizes and ranges of secondary craters around 12 different primary craters on Mercury, the Moon, and Mars, and applied the ballistic equation and crater-scaling relationships to find the size and velocity of each ejected fragment. Inferred ejecta fragments from the Moon and Mars were often large (hundreds of meters to kilometer sized) and had flown quite far (velocities ~0.5–1 km/sec). The cumulative mass of these secondary fragments was always found to be less than a few percent of the total ejected mass of the primary crater, consistent with the predictions of Melosh (1984, 1985) who suggested that most secondaries were caused by spallation of a near-surface layer near the impact site. The large fragments produced by this spallation mechanism were assumed to be clusters of small bodies with very low relative velocities rather than solid bodies. Vickery (1987) then fit a power-law function ($d = CV^{-\beta}$, where d is the size of the fragment, V is impact velocity, β is the velocity exponent derived from the data, and C is a constant) to the ejecta size–velocity data, but the 1-sigma uncertainties in the β values were often large. Moreover, secondary craters formed from high velocity fragments (>1 km/sec) are very difficult to detect; high ejection velocities cause fragments to travel into regions covered with background craters and to form non-distinctive round craters upon impact. Thus, Vickery's formula is generally too uncertain to extrapolate to higher velocities.

We only apply her formula to the case of the Moon, where we need to extrapolate from Vickery's data the least (i.e., only extending from her lower limit near 1 km/sec out to the Moon's escape velocity of 2.4 km/sec). Since lunar craters formed over the past 10–20 Myr are unlikely to be large, we examine the smallest crater tested by Vickery (1987), i.e., the lunar impact crater Harpalus (39 km). For this case, the best-fit parameters for the ejecta size–velocity relation was

$$d = 1.49 \times 10^6 V^{-1.39\pm0.2}. \quad (5)$$

Vickery also approximated the total volume of the secondary ejecta from Harpalus to be 4.24×10^8 m^3 and the ratio of the high velocity spall volume to the total volume of the secondary ejecta to be 2×10^{-4}. Thus, by using this data and converting (5) into a cumulative mass–velocity distribution, one can estimate the total volume of spalled material which reaches lunar escape velocity. Our results for Harpalus suggest that only a few hundred 10-m objects (at most) could have been ejected from the impact site, making it unlikely that a large S-SEA population could have come recently from the Moon. Further constraints on planetary ejecta from secondary crater data will require a new survey.

IV.B. Constraints from the Meteorite Record

Impact events on the Moon or Mars may produce meteorites by ejecting small fragments which reach Earth before they disrupt or by ejecting large fragments which reach Earth after comminuting several times. Accordingly, lunar or martian metorites may provide a constraint on whether planetary ejecta fragments 10 m in diameter or larger can or cannot be spalled from a planetary surface. We already know that lunar or martian meteorites are under-represented in the meteorite record (~20 out of >2000 meteorites), implying that few planetary ejecta fragments exist among the NEA population. We investigate whether the physical characteristics of these meteorites are consistent with either scenario.

Constraints from SNC meteorites. We find that the physical characteristics of the SNC meteorites do not conclusively show that they are fragments comminuted from a population of large-body Mars ejecta or fragments ejected recently from smaller impact events of the younger martian terrain:

1. Most SNC meteorites show little to no signs of extensive shock damage, suggesting that these objects (or their parent bodies) were spalled off Mars by shock wave interference during a impact cratering event (Melosh 1989).
2. Nine of the ten SNC meteorites are large and composed of strong mafic material (Warren 1994). (The tenth SNC, recently discovered ALH84001, is a orthopyroxene (Swindle *et al.* 1994)). Their size and strength are consistent with bodies surviving the passage from Mars to Earth. Their composition is also consistent with a scenario suggesting that at least 9 of these SNCs had a common provenance, though Treiman (1995) suggests that S and NC have followed separate histories.
3. The SNCs show isotropic radiation damage only, consistent with their remaining deep within bodies large enough to protect interior material from cosmic rays during their dynamical evolution to an Earth-crossing orbit, until they were liberated as small enough bodies (< meter-sized) to be isotropically irradiated. On the other hand, the SNCs may have been ejected as small bodies who quickly arrived at Earth via a high ejection velocity or through transport within a chaotic resonant zone (Gladman and Burns 1995).
4. Cosmic-ray exposure ages for the SNC meteorites clusters into several groups: 0.8, 3.1, 13, 15, and 16 Myr (Warren 1994, Swindle *et al.* 1994). These ages may represent the transit time spent between liberation and Earth impact, where the groups may indicate various impact liberation events. On the other hand, these cosmic-ray exposure ages may reflect direct transport times from Mars to Earth via a chaotic resonant zone.
5. The SNCs igneous cystallization ages, though controversial, suggest they are ~180 Myr old (McSween 1994).

This young age and the SNCs mafic nature implies ejection from the young terrain on Mars. However, few large craters capable of ejecting meter-sized fragments exist on young martian terrain (Vickery and Melosh 1987). To solve this problem, McSween (1994) and Treiman (1995) suggested that the SNCs were ejected by a small cratering event ~10 Myr ago (corresponding to the longest CRE ages) on the young terrain and that only meter-sized fragments were ejected. Recent dynamical results from Gladman and Burns (1995) show that secular resonances could transport the SNCs to Earth-crossing orbits within 1 Myr. On the other hand, Vickery and Melosh (1987) claim that if smaller martian craters had launched the SNCs, we would expect to see 5 to 6 times as many old meteorites as young ones produced by craters of similar magnitude on the old terrain of Mars. An alternative scenario, suggested by Vickery and Melosh (1987), has the SNCs ejected from a single 100 km crater ~200 Myr ago as part of ejecta fragments >6 m in diameter. Such an event would bury the region under an ejecta blanket around it for hundreds of kilometers, disguising the young igneous terrain. They claim that the probability of a 100 km impact over the past ~200 Myr is nearly 100%.

6. The recovered mass of the SNC meteorites is 100 times larger than that of the lunar meteorites (Vickery and Melosh 1987) (e.g., all lunar meteorites have masses below 1 kg, while the SNCs have four >1 kg; Warren 1994). This large difference is surprising, given that dynamical arguments suggest that the mass yield should be in favor of lunar meteorites by a factor of 2500 (Wetherill 1984), though these statistics may need revision (Gladman and Burns 1995). Vickery and Melosh (1987) explained this difference using their single 100 km crater SNC ejection event scenario: (a) the mass yield of meteorites from a single large crater is expected to be much greater than from several smaller craters (e.g., McSween's (1994) scenario described in point 5), (b) the Moon shows no evidence for a large impact within the past 10–20 Myrs, and (c) (as discussed below) there are several lines of evidence that suggest that lunar meteorites come from small impact events.

Constraints from lunar meteorites. The physical characteristics of lunar meteorites suggest they were never part of an evolving population of large bodies such as the S-SEAs, but rather were ejected directly to Earth by small cratering events spread over the surface of the Moon (Warren 1994, Gladman *et al.* 1995). The key constraining properties are:

1. The ten lunar meteorites (including pairs) are composed of weak regolith breccias with most having CRE ages less than 1 Myr (Warren 1994), consistent with material which spends little time in transit to the Earth. Note that "weak" refers in this instance to the strength of a meteorite entering the Earth's atmosphere, not its ability to withstand disruption in a collision in space—the porosity of breccias can absorb large amounts of shock energy and thus be "strong" as well. (D. Kring, personal communication).

2. Lunar meteorites appear to have been exposed to both hemispheric (2π steradian) radiation (while within a few meters of the surface of their parent body or the Moon) and isotropic (4π) radiation (as small bodies after ejection from their parent body or the Moon), consistent with excavation by small cratering events (Warren 1994).

3. The petrology of the lunar meteorites suggests they are from a variety of sources spread across the Moon, rather than from a single impact site (Warren 1994).

4. The lunar meteorites are all small. If large lunar fragments dominated the S-SEA population, we would expect to see several lunar meteorites with similar petrologic characteristics, as we do with the SNC meteorites.

V. CONCLUSIONS

We summarize our model's key results below:

• Main-belt fragments generally do not evolve into the low-e orbits needed to produce the S-SEAs. Instead, most lie along the $q = 1$ AU line up to the 3:1 resonance where Spacewatch would detect a large fraction of them (if they existed).

• Ejecta from Mars provides a marginal fit to the dynamical constraints of the S-SEAs; they fail to match S-SEAs with high inclinations. However, secular resonances not included in this model can increase asteroid inclinations (Gladman and Burns 1995).

• Ejecta from the Earth, Moon, and Venus provide a marginal to poor fit to the dynamical constraints of the S-SEAs. They high fail to match any of the S-SEAs with $i > 14°$. They also produce large residence time contours along the $Q = 1$ AU line, inconsistent with the current S-SEAs population, though inaccurate observational selection effects may be responsible. Cratering constraints make it unlikely that the S-SEAs were formed within the clearing time for material on low-e Earth-crossing orbits (~10–20 Myr). Lunar meteoritical constraints also lower the likelihood that the Moon was a substantial source for the S-SEAs.

• Stochastic disruptions of near-Earth asteroids provide a poor fit to the dynamical constraints of the S-SEAs. Multiple asteroid disruption events in the low-e Earth-crossing orbit region over the dynamical clearing time of 10–20 Myr are unlikely. Single asteroid disruption events yield a narrow range of orbital inclinations, inconsistent with the observed S-SEAs.

• Test bodies evolving from low eccentricity Amor asteroid-class orbits beyond the $q = 1$ AU line provide the best fit the dynamical and physical constraints of the S-SEAs.

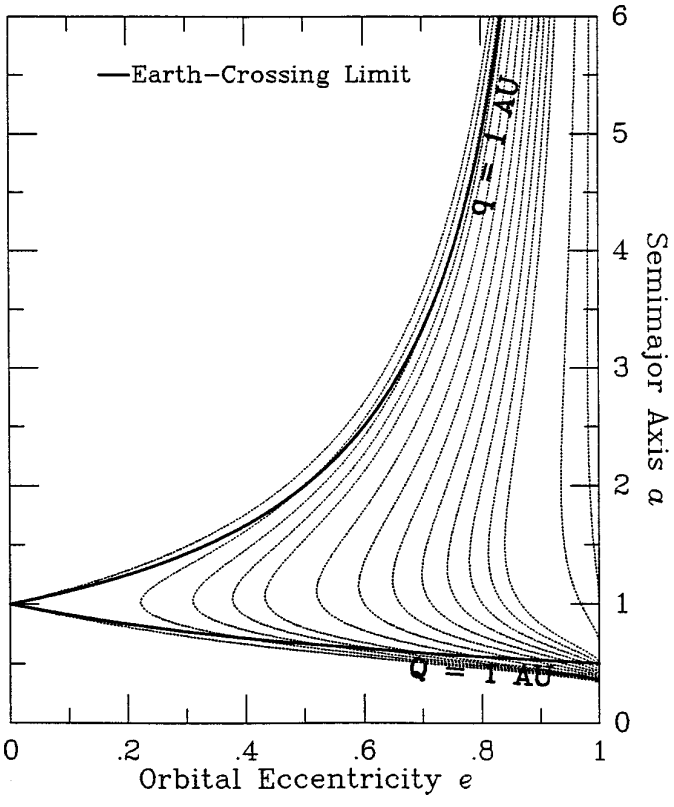

FIG. A1. Figure showing the lines of constant Tisserand invariant (see Eq. 2.2) as a function of a and e, where $i = 0$. The contours are (from left to right) T = (3.0, 2.95, 2.9, 2.85, 2.8, 2.7, 2.6, 2.5, 2.4, 2.3, 2.2, 2.1, 2.0, 1.5, and 1.0. (Figure from Greenberg and Nolan 1993).

APPENDIX A: NEA DYNAMICAL EVOLUTION PATHS

The orbital motions of near-Earth asteroids (NEAs) follow well-known evolutionary paths that have been characterized by Greenberg and Nolan (1989, 1993). In this appendix, we briefly summarize their description as follows, because it lays the groundwork for the research described in this paper.

One constraint on the motion of a NEA comes from the Jacobi integral of the restricted three-body problem, where the Sun, Earth, and the asteroid are the three bodies considered. The Jacobi integral limits the motion of test bodies to those surfaces in (a, e, i) space allowed by each body's angular momentum and orbital energy. Thus, even though a planetary encounter may drastically modify a body's orbital elements, its new motion must still adhere to the same Jacobi integral constraints as those given before encounter. These surfaces in (a, e, i) space can be characterized by the "Tisserand invariant" T, which describes the pseudo-energy of each body that must be conserved:

$$T \equiv \frac{1}{a} + 2\,[a(1 - e^2)]^{1/2} \cos i. \qquad (6)$$

Using these constraints, Greenberg and Nolan approximated the orbital evolution of an Earth-crosser exiting a main-belt resonance by assuming its orbit was modified solely by the Earth's gravitational force. The other planets were considered negligible perturbers for this approximation; they are either too small (e.g., Mars) or too far away (e.g., Jupiter, Venus, Mercury). They also assumed that the eccentricity of the Earth is zero. These simplifications allowed them to use the Tisserand invariant to display the restricted surfaces in (a, e) space for this system at any chosen inclination. Figure A1 shows T values for an inclination of 0°.

Typical NEA orbits change very little between Earth encounters. However, Earth encounters themselves can significantly modify NEA orbits, though the new orbit is constrained to a surface of constant T. A similar family of curves exists for each perturbing planet (Mercury–Jupiter). The Monte Carlo code assumes that a given NEA random walks along a surface of constant T, with its largest step in (a, e) space corresponding to the largest ΔV kick given by a planet. These paths are shown in Fig. A2.

Main-belt material in resonance that reaches the perihelion $q = 1$ AU line random walks along the contours of constant Tisserand invariant following near that line (Fig. A1). Some of this material may even survive long enough to follow these same contour lines "around the bend" to approach the $Q = 1$ AU line. Typical dynamical evolution along these contours lasts 1–10 Myr. Other dynamical paths can be generalized to Mars, in which asteroids, which are solely Mars-crossing, follow Tisserand surfaces set by the orbital parameters and gravitational acceleration of Mars. However, Mars has a substantial eccentricity, making such curves very rough approximations. Dynamical evolution for solely Mars-crossing bodies parallels the evolution of NEAs, although the time scales are much longer.

Once a NEA becomes Venus-crossing as well as Earth-crossing it

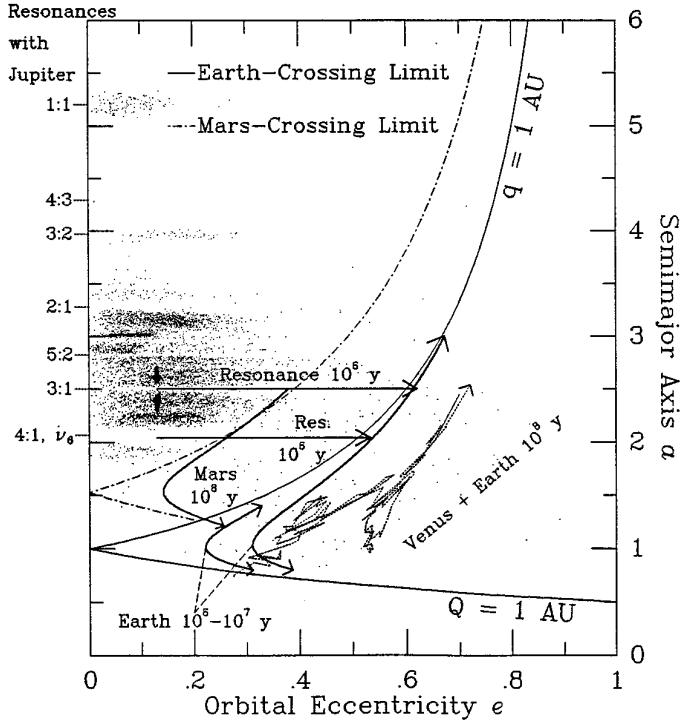

FIG. A2. Figure showing the dynamical paths that can deliver asteroids from the main-belt to Earth-crossing and then loss from Earth-crossing. The arrows show the paths of the objects described in the text. The short vertical arrows in the main belt represent collision injection into the resonances, the horizontal arrows represent the perturbations by resonances, and the curved arrows represent the perturbations due to planetary encounters. The jagged arrow shows the ejection path of a sample test body perturbed by Venus and Earth into a Jupiter-crossing orbit. Asteroids crossing Jupiter's orbit are frequently ejected from the Solar System (Figure from Nolan 1994).

no longer is constrained to constant T lines. Since Venus gravitational acceleration is comparable to Earth's, the single perturber hypothesis breaks down. Subsequent encounters from Earth and Venus allow the NEA to freely wander (a, e, i) space. Eventually, asteroids experiencing repeated close approaches with the terrestrial planets may dynamically evolve into Jupiter-crossing orbits, which are quickly ejected from the Solar System (~1 Myr).

NEAs can follow other paths not dominated by perturbations from the terrestrial planets. Deviations from the Tisserand invariant contours occur when the effects of a non-zero eccentricity of a planet are magnified by some resonance. Moreover, new results from Farinella *et al.* (1994) suggest that many objects in the ν_6 secular resonance can quickly become sun-grazing (e.g., ~1 Myr) if (terrestrial) planetary perturbations do not first remove them from resonance. In terms of Fig. A2, these objects follow a horizontal path from the ν_6 resonance to either a Jupiter-crossing orbit, where they are removed from resonance by Jupiter perturbations, or all the way to $e \sim 1.0$, where they collide with the Sun. Although the importance of this path needs to be further quantified, it appears that some main-belt material from this path may add to the high-eccentricity population of objects comprising the Jupiter comet family and the Taurid meteoroid complex (Valsecchi *et al.* 1994).

ACKNOWLEDGMENTS

We thank Don Davis, Dan Durda, Brett Gladman, Ellen Howell, Robert Jedicke, Dave Kring, Jean-Marc Petit, David Rabinowitz, and Jim Scotti for their helpful discussions and suggestions, and for providing useful critiques of this paper throughout the past year. We also thank Paolo Farinella and Alessandro Morbidelli for their thoughtful and constructive reviews which made this paper stronger and more balanced. Finally, we thank David Rabinowitz for the use of his observational bias correction functions and Jean-Marc Petit for the use of his asteroid fragmentation code (in conjunction with Paolo Farinella). This work was supported by Grant NAGW-1029 from NASA's Planetary Geology and Geophysics Program.

REFERENCES

Arnold, J. R. 1965. The origin of meteorites as small bodies. II. The model. *Astrophys. J.* **141,** 1536–1547.

Belton, M. J. S. and 19 colleagues. 1992. Galileo encounter with 951 Gaspra: First pictures of an asteroid. *Science* **257,** 1647–1652.

Bottke, W. F. 1995. *The Collisional and Dynamical Evolution of Asteroids.* Ph.D. Dissertation, Department of Planetary Sciences, University of Arizona.

Bottke, W. F., M. C. Nolan, R. Greenberg, and R. A. Kolvoord 1995. Collisional lifetimes and impact statistics of near-Earth asteroids. In *Hazard Due to Comets and Asteroids* (T. Gehrels, M. S. Matthews, Eds.) pp. 337–357. Univ. of Arizona Press, Tucson.

Bottke, W. F., M. C. Nolan, and R. Greenberg 1994. Velocity distributions among colliding asteroids. *Icarus* **107,** 255–268.

Bottke, W. F., and R. Greenberg 1993. Asteroidal collision probabilities. *Geophys. Res. Lett.* **20,** 879–881.

Davis, D. R., E. V. Ryan, and P. Farinella 1994. Asteroid collisional evolution: Results from current scaling algorithms. *Planet. Space Sci.* **42,** 599–610.

Dohnanyi, J. S. 1969. Collisional model of asteroids and their debris. *J. Geophys. Res.* **74,** 2531–2554.

Dones, L., B. Gladman, H. J. Melosh, H. F. Levison, and M. J. Duncan 1995. Dynamical lifetimes of small bodies: Orbit integrations vs Öpik calculations. *Bull. Am. Astron. Soc.* **27,** 1073.

Everhart, E. 1985. An efficient integrator that used Gauss-Radau spacings. In *Dynamics of Comets: Their Origin and Evolution* (A. Carusi and G. B. Valsecchi, Eds.), pp. 185–235. D. Reidel, Dordrecht, Holland.

Farinella, P., Ch. Froeschlé, Cl. Froeschlé, R. Gonczi, G. Hahn, A. Morbidelli, and G. B. Valsecchi 1994. Asteroids falling into the sun. *Nature* **371,** 314–317.

Farinella, P., and D. R. Davis 1994. Why are small Earth-approachers different? *Bull. Am. Astron. Soc.* **263,** 1167.

Farinella, P., R. Gonczi, Ch. Froeschlé, and Cl. Froeschlé 1993. The injection of asteroid fragments into resonances. *Icarus* **101,** 174–187.

Froeschlé, Ch., G. Hahn, R. Gonczi, A. Morbidelli, and P. Farinella 1995. Secular resonances and the dynamics of Mars-crossing and near-Earth asteroids. *Icarus* **117,** 45–61.

Gladman, B., and J. A. Burns 1995. Meteorites from Mars and Mercury (yes and probably no). *Bull. Am. Astron. Soc.* **27,** 1074.

Gladman, B., J. A. Burns, M. J. Duncan, and H. Levison 1995. The dynamical evolution of lunar impact ejecta. *Icarus* **118,** 302–321.

Greenberg, R., and M. C. Nolan 1993. Dynamical relationships of near-Earth asteroids to main-belt asteroids. In *Resources of Near-Earth Space* (J. Lewis, M. S. Matthews, and M. L. Guerrieri, Eds.), pp. 473–492. Univ. of Arizona Press, Tucson.

Greenberg, R., and M. C. Nolan 1989. Delivery of asteroids and meteorites to the inner solar system. In *Asteroids II* (R. P. Binzel, T. Gehrels, and M. S. Matthews, Eds.), pp. 778–804. Univ. of Arizona Press, Tucson.

Greenberg, R., A. Carusi, and G. B. Valsecchi 1988. Outcomes of planetary close encounters: A systematic comparison of methodologies. *Icarus* **75,** 1–21.

Housen, K. R., and K. A. Holsapple 1990. On the fragmentation of asteroids and planetary satellites. *Icarus* **84,** 226–253.

Jopek, T. K., P. Farinella, Ch. Froeschlé, and R. Gonczi 1995. Long-term dynamical evolution of the brightest bolides. *Astron. Astrophys.* **302,** 290–300.

McSween, H. Y. 1994. What have we learned about Mars from SNC meteorites. *Meteoritics* **29,** 757–779.

Melosh, H. J. 1989. *Impact Cratering*: *A Geologic Process.* Oxford Univ. Press, New York.

Melosh, H. J. 1985. Ejection of rock fragments from planetary bodies. *Geology* **13,** 144–148.

Melosh, H. J. 1984. Impact ejection, spallation, and the origin of meteorites. *Icarus* **59,** 234–260.

Melosh, H. J., and W. B. Tonks 1993. Swapping rocks: Ejection and exchange of surface material among the terrestrial planets. *Meteoritics* **28,** 398.

Michel, P., Ch. Froeschlé, and P. Farinella 1996. Dynamical evolution of NEAs: Close encounters, secular perturbations, and resonances. In *Worlds in Interaction—Small Bodies and Planets of the Solar System* (H. Rickman and M. J. Valtonet, Eds.) 151–164, Kluwer, Dordrecht.

Milani, A., M. Carpino, and F. Marzari 1990. Statistics of close approaches between asteroids and planets: Project SPACEGUARD. *Icarus* **88,** 292–335.

Morrison, D. (Ed.) 1992. *The Spaceguard Survey. Report of the NASA near-Earth object detection workshop.* NASA, Washington, D.C.

Nolan, M. C. 1994. *Delivery of Meteorites from the Asteroid Belt.* Ph.D. Dissertation, Department of Planetary Sciences, University of Arizona.

Nolan, M. C., and W. F. Bottke 1995. Orbital evolution of the Spacewatch small Earth-approaching asteroids. *Bull. Am. Astron. Soc.* in press.

Öpik, E. J. 1951. Collisional probabilities with the planets and the distribu-

tion of interplanetary matter. *Proc. Roy. Irish Acad.* **A54,** 165–199. (See also Öpik 1976. *Interplanetary Encounters*. Elsevier, Amsterdam.)

Petit, J-M, and P. Farinella 1993. Modelling the outcomes of high-velocity impacts between small solar system bodies. *Celest. Mech. Dynam. Astron.* **57,** 1–28.

Rabinowitz, D. L. 1994. The size and shape of the near-Earth asteroid belt. *Icarus* **111,** 364–377.

Rabinowitz, D. L. 1993. The size distribution of the Earth-approaching asteroids. *Astrophys. J.* **407,** 412–427.

Rabinowitz, D. L., T. Gehrels, J. V. Scotti, R. S. McMillian, M. L. Perry, W. Wisniewski, S. M. Larson, E. S. Howell, and B. E. A. Mueller 1993. Evidence for a near-Earth asteroid belt. *Nature* **363,** 704–706.

Rubincam, D. P. 1995. Asteroid orbital evolution due to thermal drag. *J. Geophys. Res.* **100,** 1585–1594.

Swindle, T. D., M. K. Burkland, and J. A. Grier 1994. Noble gases in ALH84001: Not just another SNC. *Meteoritics* **29,** 538.

Treiman, A. H. 1995. S ≠ NC: Multiple source areas for martian meteorites. *J. Geophys. Res.* **100,** 5329–5340.

Valsecchi, G. B., A. Morbidelli, R. Gonczi, P. Farinella, Ch. Froeschle, and Cl. Froeschle 1994. The dynamics of objects in orbits resembling that of P/Encke. *Icarus* **118,** 169–180.

Van Houten, C. J., I. Van Houten-Groenveld, P. Herget, and T. Gehrels 1970. The Palomar-Leiden survey of faint minor planets. *Astron. Astrophys. Suppl.* **2,** 339–448.

Vickery, A. M. 1987. Variation in ejecta size with ejection velocity. *Geophys. Res. Lett.* **14,** 726–729.

Vickery, A. M. 1986. Size-velocity distribution of large ejecta fragments. *Icarus* **67,** 224–236.

Vickery, A. M., and H. J. Melosh 1993. Origin of Rabinowitz objects: Constraints from orbital evolution models. *Meteoritics* **28,** 453.

Vickery, A. M., and H. J. Melosh 1987. The large crater origin of SNC meteorites. *Science* **237,** 738–743.

Warren, P. H. 1994. Lunar and martian meteorite delivery services. *Icarus* **111,** 338–363.

Wetherill, G. W. 1988. Where do the Apollo objects come from? *Icarus* **76,** 1–18.

Wetherill, G. W. 1985. Asteroidal source of ordinary chondrites. *Meteoritics* **20,** 1–22.

Wetherill, G. W. 1984. Orbital evolution of impact ejecta from Mars. *Meteoritics* **19,** 1–12.

Wetherill, G. W. 1967. Collisions in the asteroid belt. *J. Geophys. Res.*, **72,** 2429–2444.

Wetherill, G. W., and D. O. ReVelle 1981. Which fireballs are meteorites? A study of the Prairie Network photographic meteor data. *Icarus* **48,** 308–328.